JVGR review paper

Exsolved Volatiles in Magma Reservoirs

Marie Edmonds[1*] and Andrew W. Woods[1,2]

1 Earth Sciences Department, University of Cambridge, Downing Street, Cambridge CB2 3EQ, UK

2 BP Institute, Bullard Laboratories, Madingley Rd, Cambridge CB3 0EZ, UK

*Corresponding author, marie.edmonds@esc.cam.ac.uk

Abstract

We review our understanding of the exsolved volatile phase co-existing with magmas during pre-eruptive storage at the pressures and temperatures corresponding to crustal magma reservoirs. We explore the consequences and implications of such a volatile phase for magma and ore body petrogenesis and the fluid dynamics of magma reservoirs. We outline the geochemical constraints on the size and composition of the exsolved volatile phase that may co-exist with magmas in the crust. We distinguish between decompression-driven and crystallization-driven exsolution, and describe the implications of the volatiles for the dynamics of the magma reservoir, using key natural examples and case studies. We discuss eruptions triggered by second boiling, and the various regimes of magma mixing and magma overturn that may be induced by second boiling in a layered reservoir. We also explore the control of the volatile content of the magma on the mass erupted during an eruption episode, and compare our models to eruption datasets. We then turn to the mechanisms for magma-volatile separation, noting that in crystal-poor melts convective separation of exsolved volatiles may dominate while in crystal-rich melts, volatiles may generate channels or permeable-flow pathways through the crystal mush, thereby separating from the parent magma. We discuss the implications of the accumulation of the exsolved volatile phase at the roof zones of crystal-rich reservoirs for the large gas emissions observed during explosive eruptions, and for the development of metal-rich porphyry deposits.

1. Introduction

Magmas close to the surface of Earth, stored within crustal reservoirs, contain exsolved volatiles. This exsolved volatile phase is made up of water and carbon dioxide primarily, but also significant amounts of sulfur and halogen gases, and trace constituents such as volatile metals (Gerlach, 1980; Symonds et al., 1994). These volatiles are dominantly sourced from the mantle, but may also also be assimilated from crustal rocks and fluids (Mason et al., 2017) and are enriched in silicate melts as they cool and fractionate. Typically, basaltic melts leave the mantle carrying 0.1-4 wt% H_2O and <2 wt% CO_2, depending on tectonic setting (Blundy et al., 2010; Plank et al., 2013; Wallace, 2005), which increases due to fractionation prior to volatile saturation, reaching several wt% H_2O for magmas in arc settings (Plank et al., 2013; Sisson and Layne, 1993). These volatile species have a propensity to exsolve or partition into a low density exsolved volatile phase at crustal pressures, which may be a supercritical fluid at high pressures, and a vapour phase at low pressures.

Despite only being a minor constituent of magmas, exsolved volatiles have enormous importance for a myriad of magma reservoir processes. An exsolved volatile phase lowers the bulk density and increases the buoyancy of magmas (Anderson, 1995), influences phase equilibria (Ghiorso and Gualda, 2015; Moore and Carmichael, 1998), as well driving convection (Cardoso and Woods, 1999; Longo et al., 2006) and promoting magma mingling and mixing through overturn (Huppert et al., 1982; Ruprecht et al., 2008). Recent work has shown that the exsolved volatile phase may be mobile in crystal-rich magma (Barth et al., in review; Oppenheimer et al., 2015; Parmigiani et al., 2016), leading to accumulation in the roof zones of magma reservoirs, which may play a role in triggering eruptions, activating hydrothermal systems through volatile injection (Chiodini et al., 2012) and in the generation of porphyries hosting economic concentrations of metals (Guo and Audétat, 2017; Huber et al., 2012).

Important new advances in observing and modeling magma reservoirs and their volatile systematics have prompted this review. Our understanding of the form and organisation of crustal magma reservoirs has evolved in recent years, towards a picture of trans-crustal, mush-dominated, heterogeneous magma reservoirs which may be long-lived relative to inter-eruption timescales (Cashman et al., 2017; Cooper and Kent, 2014). Petrological evidence, from melt inclusion and pyroxene barometry (Edmonds et al., 2016; Hartley et al., 2014; Longpré et al., 2017; Métrich and Wallace, 2008; Neave and Putirka, 2017) suggests that magmas may be stored over a wide depth interval and that the magmas typically carry crystal cargos that record complex mixing and mingling histories (Cashman and Blundy, 2013; Cooper and Kent, 2014; Costa et al., 2013; Neave et al., 2013), suggesting repeated recharge and mixing of localised melts and mushes. Geophysical surveys of the crust show that melt-dominated magma bodies do not generally exist; instead it is envisaged that melts are disseminated in mushes or in closely-spaced sill-like bodies (Cordell et al., 2018; Kiser et al., 2016; Pritchard and Gregg, 2016).

Large fluxes of deep-derived sulfur-rich gas from long-lived eruptions such as Soufrière Hills Volcano (Montserrat) (Christopher et al., 2015; Edmonds et al., 2010; Edmonds et al., 2001) and Bagana Volcano (Papua New Guinea) (Kilbride et al., 2018), which continue during prolonged eruptive pauses indicate that permeable, outgassing pathways through crystal-rich magma may be maintained from depth, perhaps tapping zones where an exsolved volatile phase accumulated near the topmost regions of the magma reservoir system over multiple eruption timescales (Christopher et al., 2015), with the system being recharged from time to time with heat and volatiles by underplating mafic magmas (Bachmann and Bergantz, 2006; Murphy et al., 2000;

Plail et al., 2014). The accumulation of an exsolved volatile phase in the roof zone of such a protracted reservoir may play a critical role in triggering and sustaining eruption. Observations of "excess sulfur" using space-borne satellites (Carn et al., 2016; Wallace, 2001) may be direct evidence of such deep accumulations of exsolved volatiles. Large volcanic "outgassing events" which may be observed using strain measurements (Hautmann et al., 2014), may relieve reservoir pressure and prevent magmatic eruptions. Accumulation of an exsolved volatile phase may also have important implications for the interpretation of ground displacements at the surface through the formation of a highly compressible region of the magma reservoir (McCormick Kilbride et al., 2016; Rivalta and Segall, 2008), which may buffer volume changes and suppress ground deformation.

This review will be concerned with both the geochemistry and physical dynamics of the exsolved volatile phase in the crust prior to eruption. We bring together geochemical and physical perspectives to review the state of the art in our understanding of the role and behaviour of volatiles in magma reservoirs and during magma ascent and eruption. We provide a synopsis of recent progress in this area in the key areas of observation, modeling and experiment and highlight outstanding, critical problems that remain to be solved.

2. Achieving volatile saturation in magmas

Magmas exsolve water and carbon dioxide as they rise through the crust, cool and crystallise. Owing to the relationship between volatile solubility and pressure (Dixon et al., 1995; Moore et al., 1998a; Newman and Lowenstern, 2002; Pan et al., 1991; Stolper and Holloway, 1988), melts can reach saturation with respect to an exsolved volatile phase during decompression (termed "first boiling") or during isobaric cooling and crystallisation (of volatile-poor crystals) in a magma storage area ("second boiling") (**figure 1A and B**), leading to the formation of a exsolved magmatic volatile phase (MVP) (Candela, 1997). A magma is said to be volatile-saturated when an exsolved volatile phase (which may be a supercritical fluid at high pressures, or a vapour at low pressures) is present and in equilibrium with the melt. Volatile exsolution occurs when the sum of the vapour pressures of the components of a liquid, $\sum\left(P_i^{vapour}\right)$, is equal to the load pressure (Candela, 1997). Volatile exsolution into bubbles will occur when either the load pressure is reduced, for example during decompression or removal of lithostatic load, "first boiling", or $\sum\left(P_i^{vapour}\right)$ is increased, for example during crystallisation, "second boiling".

Exsolution of water from silicate melt during decompression-induced degassing, or first boiling, results in a lowering of the solidus, owing to a decrease in the entropy of mixing caused by the loss of water from the melt. Decompression of magma is therefore usually accompanied by extensive degassing-induced crystallisation (Cashman and Blundy, 2000; Cashman, 2004), which has the effect of promoting further volatile exsolution and increasing the bulk viscosity of the magma (Dingwell et al., 1996). These processes are first order controls on eruption style and the onset of fragmentation (Blundy and Cashman, 2005; Dingwell, 1996; Melnik and Sparks, 2002) (see later). Second boiling takes place in magma storage areas in the crust, where magmas cool beneath their solidus temperatures and crystallise. If the fractionating assemblage is dominantly anhydrous then as the liquid fraction decreases, the vapour pressure of the volatile components increases, driving exsolution of volatiles (**figure 1B**). As magmas rise through the crust, the balance between first and second boiling changes. As magma ascent slows, volatile exsolution may be driven dominantly by cooling and crystallisation; whereas rapid rise of magma through dykes to the surface will experience dominantly first boiling vesiculation and expansion. For the case of large, complex magma reservoirs which evolve over long timescales (10^4-10^5 yr) (Cooper and Kent, 2014; Hawkesworth et al., 2000) the production of an exsolved volatile phase may occur sporadically, with magma recharge events, superimposed on a background of slower exsolved volatile production driven by cooling and crystallisation.

The composition of the evolving exsolved magmatic volatile phase will depend on the initial volatile content of the magma, the pressure, temperature, melt composition and oxidation state. There have been many recent formulations of empirical (Moore et al., 1998b) and thermodynamic (Burgisser et al., 2015; Dixon and Stolper, 1995; Moretti et al., 2003; Papale, 1999; Witham et al., 2012) models to describe the chemical evolution of melt and exsolved volatile phase in equilibrium during transit through the crust (**figure 2**). The thermodynamic models are calibrated by experimental data on H_2O and CO_2 solubility and the partitioning of sulfur between the aqueous exsolved volatile phase and silicate melt at a range of conditions. **Figure 2** illustrates the effect of CO_2 on the composition and pressure at which volatile-saturation occurs (Candela, 1997). One melt with 400 ppm CO_2 and around 2 wt% H_2O crystallises at a constant pressure of 200 MPa. Initially it is 'vapor'-undersaturated (here 'vapor' refers to the exsolved volatile phase), but reaches vapor-saturation after around 50% crystallization (red dot in **figure 2**). At this stage the concentrations of H_2O and CO_2 have approximately doubled and $\sum\left(P_i^{vapour}\right)$ is 200 MPa, and the partial pressures of H_2O and CO_2 are both ~ 100 MPa and therefore the molar proportions of CO_2 and H_2O in the co-existing exsolved volatile phase are

approximately equal. Further vapor-saturated crystallization will cause the melt to evolve along the 200 MPa isobar, towards more H_2O-rich melt compositions. If no CO_2 were present (**figure 2**, bottom orange dot), then 64% crystallization is required before vapor-saturation occurs. **Figure 3** shows the relationship between the melt H_2O content, the mass of the exsolved volatile phase and the degree of crystallization at 200 MPa for a range of initial water contents. After 50% crystallization, by which time basalt has become basaltic andesite, 1-5 wt% exsolved volatiles is likely to co-exist with the melt. This is a minimum estimate; if CO_2 is present this fraction will be higher. Many authors have suggested that magmas may experience 'CO_2-flushing' which will tend to drive the melt towards higher CO_2 concentrations (from right to left along an isobar in **figure 2**) (Caricchi et al., 2018).

2.1. Volatiles in natural magmatic systems

Perhaps our best source of information regarding the pre-eruptive volatile concentrations of silicate melts are given by the volatile contents of melt inclusions (Kent, 2008; Lowenstern, 1995; Métrich and Wallace, 2008; Sides et al., 2014b). We now understand, however, that many processes modify the concentrations of volatiles in melt inclusions post-entrapment, such as sequestration of CO_2 into a shrinkage bubble (Esposito et al., 2014; Moore et al., 2015; Wallace et al., 2015), perhaps driven by cooling and post-entrapment crystallization (Sides et al., 2014a; Steele-Macinnis et al., 2011), diffusive loss (Bucholz et al., 2013; Gaetani et al., 2012; Lloyd et al., 2013) or gain (Hartley et al., 2015) of hydrogen. A dataset of melt inclusion CO_2 and H_2O data, for A) a range of basalts in hotspot and arc settings and B) andesites, dacites and rhyolites in arc and rift settings, is shown in **Figure 4.** The data for both the mafic magmas and the more evolved magmas show an array in volatile concentrations, caused by a combination of factors such as decompressional degassing concurrent with melt inclusion entrapment and CO_2 fluxing (Métrich and Wallace, 2008), mixing (Dixon et al., 1991) and volatile loss from the inclusions (Gaetani et al., 2012; Maclennan, 2017). A degassing path is one whereby CO_2 is lost at high pressure, followed by H_2O at low pressure (Dixon and Stolper, 1995). The dissolved volatile data for both basalts and rhyolites, in all tectonic settings, is consistent with volatile-saturation at pressures of up to 300 Mpa or more in the crust, equivalent to 11-13 km depth. For ocean island magmas, the exsolved volatile phase at this depth is highly CO_2-rich, owing to the much lower bulk H_2O concentrations; in arcs, the deep exsolved volatile phase is more hydrous. If, as seems likely, the melt inclusion record is overprinted by shallow storage prior to eruption (due to H+ loss by diffusion, see above), the deeper record may be routinely erased.

Phase equilibria studies have been of value in reconstructing the pre-eruptive water contents of arc basalts (Barclay et al., 1998; Sisson and Grove, 1993). In Mexico, phase assemblages in erupted rocks are consistent with experimental assemblages under volatile-saturated conditions at 170-200 MPa (Moore and Carmichael, 1998), indicating that an aqueous fluid phase with a high activity of H_2O co-existed with magma prior to eruption. Plagioclase hygrometers (Lange et al., 2009; Putirka, 2005; Waters and Lange, 2015) allow estimates of the water content of basaltic melts to be made: it has been suggested that An contents of plagioclase in arc basalts in Japan indicate pre-eruptive basaltic water contents of 3-5 wt% (Ushioda et al., 2014), which is consistent with melt inclusion studies (Kuritani et al., 2014; Rose-Koga et al., 2014). These basalts have potential to generate large amounts of an exsolved volatile phase upon evolution to higher-silica magmas. Other mineral proxies may be useful to reconstruct melt volatile concentrations. A recent study of hydrogen in the cores of orthopyroxenes erupted during vulcanian activity at Soufrière Hills Volcano were used to suggest that melt H_2O contents were 4-9 wt% prior to eruption, implying volatile-saturated magma storage at depths of up to ~12 km prior to eruption (Edmonds et al., 2016). Anorthite-rich plagioclase in xenocrysts (derived from disaggregated mushes), Al-rich melts and experimental phase equilibria were used to infer that parental basaltic andesites beneath St Kitts (Lesser Antilles) are water-rich (>9 wt%) and they crystallise over a wide pressure range (1.5 to 6.0 kbar) (Melekhova et al., 2017).

Geochemical proxies might allow reconstruction of magmatic water budgets. It has been recognised recently that high Sr/Y ratios in magmas are linked to fertility in copper (Richards, 2011). High Sr/Y ratios, for example in Tibetan post-collisional magmas, have been attributed to high magmatic water contents of >10 wt%, acting to suppress plagioclase fractionation (and hence Sr removal) during fractional crystallisation of hydrous basalt parent magma at depth (Chiaradia et al., 2012; Lu et al., 2015). These magmas have been compared to others in subduction zone settings: silicic high Sr/Y andesites and dacites at Mount Shasta, a stratovolcano in the southern Cascades, contain melt inclusions with >10 wt% H_2O which crystallised at 0.8 GPa (Grove et al., 2002). Similar experimental phase equilibria were shown for the Pinatubo dacite melt: in order to produce high Sr/Y with a starting melt composition of 16.5 wt% Al_2O_3 requires a melt water content of >10 wt% (Prouteau and Scaillet, 2003). The existence of hydrous magmas deep in the crust lends support to the notion that magma reservoirs from the mid-crust upward contain substantial fractions of exsolved water as supercritical fluid or low density vapour at lower pressures.

237 Plutonic rocks exposed at the surface, however, present only scant evidence of an exsolved
238 magmatic volatile phase, despite abundant petrological evidence of hydrous components in the
239 melt (the presence of amphibole or biotite, for example). Comb-layered quartz, with its high
240 concentrations of fluid-mobile trace elements, is found in shallow felsic intrusions associated
241 with ore bodies, and is proposed to precipitate at the wallrock-magma contact from exsolved
242 hydrous fluids at the apical regions of magma bodies (Lowenstern and Sinclair, 1996). Some
243 granite bodies and pegmatites contain miarolitic cavities made up of super-solidus minerals,
244 externally nucleated, projecting into a quasi-spherical void (Candela, 1997). These features are
245 accepted as good evidence for magmatic exsolved volatile phase saturation in plutonic igneous
246 rocks (Candela, 1997). The absence of miarolitic cavities in granites and other igneous rocks does
247 not preclude that the magma body was saturated with respect to an exsolved volatile phase; the
248 preservation of such features depends on the depth and water content of the magma, as well as
249 crystal size, and the permeability of the mush during solidification. Some of these factors will be
250 discussed further in section 5.

251 Overall the data from natural systems appear to show that magmas may be volatile-saturated
252 from depths of 9 to 12 km up to the surface in most magmatic systems, including hotspots, arcs
253 and continental rifts. There may be exceptions, however. A recent study using apatites to
254 reconstruct the volatile budget of Campi Flegrei suggested that phonolitic magma at 7 km depth
255 was volatile-undersaturated; while that stored at 3 km was volatile-saturated (Stock et al., 2016).
256 In mid-ocean ridge and hotspot settings, basaltic melts typically contain little H_2O (<1.0 wt% and
257 usually <0.5 wt%; **figure 4**); for these magmas, saturation in an exsolved fluid phase occurs in
258 the mid-crust but the fluid is initially very CO_2-rich; water does not exsolve from the melt in
259 significant quantities until the magma is within a few hundred metres of the surface (Newman
260 and Lowenstern, 2002); or until after significant amounts of isobaric crystallization has taken
261 place.
262
263 *2.2. Sulfur partitioning into an exsolved volatile phase*
264 As well as the primary volatile species, H_2O and CO_2, sulfur is also present at bulk
265 concentrations of up to 0.5 wt% in arc magmas (Carroll and Rutherford, 1985; Jugo, 2009;
266 Metrich and Clocchiatti, 1996; Wallace and Edmonds, 2011). Sulfur has significance owing to its
267 ability to complex with metals in the magmatic exsolved volatile phase and transport them to
268 sites of ore deposits (Botcharnikov et al., 2010; Zajacz and Halter, 2009); but also because
269 "excess" sulfur emissions during large explosive volcanic eruptions may lead to tropospheric
270 cooling owing to the influence of sulfate aerosols on the radiation budget of Earth's atmosphere

(Robock, 2000). It has long been observed that the mass of sulfur released, as observed using satellite sensors, from intermediate, i.e. andesite, dacite, eruptions in arcs is far larger than can be accounted for by the syn-eruptive degassing of melt, as deduced from the sulfur content of melt inclusions (Wallace, 2001; Wallace and Gerlach, 1994). A solution to this conundrum emerged after the 1984 El Chichon eruption, which released 7 Tg sulfur into the atmosphere (Bluth et al., 1997). It was proposed that, prior to eruption, a large fraction of the sulfur existed in a pre-eruptive exsolved volatile phase, rich in H_2S (Luhr et al., 1984). This hypothesis gained traction with the observation of other large explosive eruptions (Wallace, 2001; Wallace and Gerlach, 1994; Westrich and Gerlach, 1992), as well as the experimental observations, which followed, that sulfur partitions strongly into aqueous exsolved volatile phase at crustal pressures for water-rich, relatively evolved magmas (Clémente et al., 2004; Keppler, 1999; Scaillet et al., 1998; Scaillet and Pichavant, 2005; Zajacz et al., 2012).

The sulfur content of an exsolved volatile phase in a magma reservoir may be estimated using a thermodynamic approach using homogeneous equilibria in the C-O-H-S system (Oppenheimer et al., 2011; Scaillet and Pichavant, 2003). An exsolved volatile phase that evolves in a magma reservoir prior to eruption is highly variable in sulfur content, dependent on fO_2, magma composition and temperature. Furthermore, in order to make the computed composition of the exsolved volatile phase match with that observed at the surface, using satellite-based methods, which has been overprinted by decompression-induced degassing, at least 1 wt% and in some cases up to 5 wt% of an exsolved volatile phase must be present in the magma reservoir. A pre-eruptive volatile phase is not required, or much less is required, to explain volcanic gas composition and output from more mafic systems (Oppenheimer et al., 2011; Scaillet and Pichavant, 2003). Large amounts of exsolved volatiles co-existing with magmas at depth will buffer the C/S ratio of volcanic gases observed at the surface.

The presence of a few wt% exsolved volatiles from thermodynamic calculations is consistent with studies of melt inclusion geochemistry and models of fractional crystallisation, which suggested that the magma reservoir that fed the Bishop Tuff was zoned with respect to exsolved volatiles, containing up to 6 wt% near the roof zone (Wallace et al., 1999). A recent study of the volcanic products of the Samalas eruption, Indonesia, which involved eruption of at least 40 km^3 and has been unmasked as the source of the mysterious 1257 sulfate spike in the ice core records (Lavigne et al., 2013) suggests exsolved magmatic volatile contents of >3 wt%, based on melt inclusion systematics and fractionation modeling (Vidal et al., 2016). Sulfur partitioning into this

water-rich exsolved volatile phase resulted in a syn-eruptive sulfur emission into the atmosphere of 79 +/- 6 Tg (Vidal et al., 2016). Studies of long-lived eruptions with well-constrained records of magma and gas fluxes, combined with melt inclusion studies, have allowed independent estimates of the proportion of exsolved volatiles present in the magma reservoir. At Soufrière Hills (Montserrat) much of the sulfur exists in a pre-eruptive exsolved volatile phase prior to eruption, which may comprise to to 2-3 wt% of the magma at 150-200 MPa (Edmonds et al., 2014b).

3. Consequences of exsolved volatiles in magma reservoirs for rheology and dynamics

The presence and production of an exsolved volatile phase in crustal magma reservoirs can lead to a number of different effects on rheology, compressibility and on eruption duration and style, depending on a range of factors, including whether the magma reservoir is sealed or open to the atmosphere, the crystal content and viscosity of the melt, and on whether the magma reservoir is composed of a single magma body or multiple bodies of melt with different composition and gas content. We first describe the changes in magma rheology that might occur when second boiling occurs (**figure 1**) in a crystal-rich magma, generating an exsolved volatile phase, manifest as disseminated fluid bubbles. We then describe the change in the pressure and density of magma in a chamber resulting from the exsolution of volatiles, associated with second boiling, assuming the mixture of melt, bubbles and crystals remains well-mixed. We then consider the effects of the relative motion of the gas phase, melt and crystals, and consider the implications of this for the dynamics of the system, including the effects of magma mixing, and observations of large volumes of erupted gas ("excess sulfur"; see section 2.2).

3.1 Magma Compressibility

In a magma that contains dissolved volatiles, cooling and crystallisation will induce saturation in an exsolved volatile phase (second boiling; as shown in **figure 1**). The exsolved volatile phase is typically of lower density than the melt phase and this process therefore leads to an increase in volume and hence pressure of the magma body as it deforms the surrounding crust. The effect of this increase in pressure may be to trigger an eruption (Blake, 1984; Tait et al., 1989) or the injection of magma to a higher level in the crust. The relation between the change in volume and the change in pressure during both the inflation and the deflation phases of the evolution of the system depends on the compressibility of the melt-volatile-crystal mixture (Huppert and Woods, 2002; Rivalta and Segall, 2008; Segall, 2013; Voight et al., 2010). With a volatile-saturated melt, the magma may be of order 10 times more compressible than a magma with no exsolved

volatiles. As a result, there may be a much greater volume of magma erupted prior to the relaxation of the reservoir pressure and closure of the conduit (Huppert and Woods, 2002; Woods and Huppert, 2003). Although the detailed calculation of the compressibility depends on the volatile solubility as a function of pressure and crystal content, it is useful to explore the predictions of a simplified model using (1a) Henry's law, (1b) a relation between the crystal content and temperature; (1c) a model of an elastic chamber with effective bulk rock compressibility (the inverse of the bulk modulus) β; and (1d) an idealized model for the density of the gas as given by the ideal gas law, which is approximately valid for shallower (upper crustal) systems.

$$n_e = n_o - sP \text{ if } n_o > sP \text{ and } n_e = 0 \text{ if } n_o < sP \tag{1a}$$

$$x = \left(1200 - T\right)\Big/250 \tag{1b}$$

$$dV = -V\beta dP \tag{1c}$$

$$1\Big/\rho = \left(n_e RT\Big/P + \left(1 - n_e\right)\Big/\rho_m\right) \tag{1d}$$

where n denotes volatile mass fraction, with subscript e denoting exsolved volatiles and o denoting the total mass of volatiles per unit mass of original melt. P is pressure and s is a solubility constant. x denotes crystal fraction (excluding the volatile phase), T temperature (in Kelvin) and V the chamber volume, while R is the ideal gas constant. The bulk density of the magma-crystal-volatile mixture is denoted by ρ while the bulk density of the melt-crystal mixture is ρ_m. Such a simplified model provides insight into the behaviour of the system and allows us to distinguish the different controlling effects on the evolution of the melt.

Combining these relations, we can calculate the compressibility (or the inverse of the bulk modulus of the mixture) defined as

$$\beta_m = -\left(1\Big/V\right)dV\Big/dP \tag{2}$$

as a function of pressure. In **figure 5a**, we illustrate the compressibility for the cases of magma with three different volatile contents at different depths in the crust, which shows that the compressibility becomes much larger once the melt reaches shallow depths where there are exsolved volatiles. The compressibility of the melt evolves as the melt cools and crystallises

367 during second boiling. In **figure 5b**, we illustrate the compressibility of magma with bulk H_2O
368 contents of 3, 4 and 6 wt % at a depth of 5 km, with the compressibility shown as a function of
369 the crystal content of the melt. Once the magma crystallises sufficiently such that the melt
370 reaches saturation in an exsolved volatile phase, the magma compressibility increases by over an
371 order of magnitude.
372
373 Magma compressibility, caused by the presence of an exsolved magmatic volatile phase in the
374 reservoir, has implications for the interpretation of volcano monitoring data and impacts the
375 magnitude of ground displacements as well as the composition and flux of volcanic gases (Biggs
376 and Pritchard, 2017; McCormick Kilbride et al., 2016). At Soufrière Hills Volcano, Montserrat
377 for example, a gas-rich compressible magma (the 'magma sponge') was invoked to explain why
378 surface displacements, measured by Global Positioning Satellite (GPS) receivers on the volcano's
379 flanks, yielded a much smaller volume displacement than the actual volume erupted, for
380 particular time periods within the eruption (1995-2011) (Voight et al., 2010). It has been
381 observed that the volume change inferred from magma chambers feeding shallower dyke
382 intrusions is often a factor of 4-5 lower than the volume increase observed in the dyke, which has
383 been explained by a combination of decompression-driven degassing and consequent increase in
384 magma compressibility, combined with the more compliant dyke geometry (Rivalta and Segall,
385 2008). A database of eruptions for which the change in volume of the chamber and the volume
386 erupted were well-constrained by the complementary data sets obtained from satellite
387 measurements of the volcano deformation and ground-based measurements of the mass erupted is
388 summarized by (McCormick Kilbride et al., 2016). They find that the volumes are generally in
389 the ratio 1-20, which indicates the presence of exsolved volatiles in the magma reservoir;
390 however, it is worth noting that it is somewhat difficult to constrain the actual change in volume
391 of the magma chamber without detailed information of the shape and depth of the chamber,
392 which can lead to changes in the effective bulk compressibility β by up to an order of magnitude
393 (Anderson and Segall, 2011; Rivalta and Segall, 2008; Segall, 2013).
394
395 *3.2. Pressure increase during second boiling*
396 Second boiling during cooling and crystallization, generating a magmatic exsolved volatile phase,
397 can produce enough pressure in the magma reservoir to trigger eruption (Blake, 1984; Tait et al.,
398 1989; Woods and Cardoso, 1997). As a simplified calculation, in a more viscous melt, the
399 pressure increase through cooling and the associated crystallization and volatile exsolution can be
400 expressed by the relation

$$\left(\beta+\beta_m\right)dP=\left(1/\rho\right)\left(d\rho/dT\right)dT=-\rho\left(nR/T+\left(sRT/P^{0.5}\right)\left(dX/dT\right)\right)dT \quad (3)$$

where the change in volume associated with the cooling and volatile expansion and exsolution is accommodated by compression of the remaining magma-volatile mixture, with compressibility β_m, and the surrounding country rock with effective compressibility β.

The predictions of this model are shown in **figure 5c** in which we see that the change in pressure per degree of cooling, relative to the critical overpressure to trigger an eruption, as a function of the crystal content of the melt. In this model, the chamber is assumed to be closed, and cooling leads to crystallisation, exsolution and deformation of the surrounding country rock. Here the critical overpressure to drive an eruption, P_c, has been set to the value 10^7 Pa (Blake, 1984; Woods and Cardoso, 1997) for illustration. It is seen that once the magma is volatile-saturated, the continued exsolution of volatiles with cooling leads to a significant expansion of the melt-crystal-volatile mixture and a large associated increase in the pressure. In the calculations shown, for magma with 3, 4 or 6 wt% H_2O, with cooling of the melt by an amount of order 10 °C, the pressure will increase up to about 10^7 Pa, leading to eruption. In contrast, if the melt is not volatile-saturated, then the increase in pressure with cooling is only associated with either the density change as melt precipitates crystals, or the bulk cooling of the melt, and these are much smaller effects.

3.3 Effect of compressibility on the mass of magma erupted

If the critical pressure to trigger an eruption from a magma reservoir is ΔP_c, where $\Delta P_c << P_l$, (where P_l is the lithostatic pressure), then the volume increase in the magma reservoir to accommodate this overpressure, relative to the lithostatic pressure, is given by $\Delta V = V\beta\Delta P_c$, based on the response of the crust. On eruption, this overpressure is relieved. The mass of melt in the chamber associated with the overpressure, ΔM, is given by

$$\Delta M = V\Delta\rho + \rho\Delta V = M\left(\beta+\beta_m\right)\Delta P_C \quad (4)$$

and this also corresponds to the mass erupted to relieve the overpressure. The volume erupted, $\Delta V_e = \Delta M/\rho$, depends on the volume change of the chamber, ΔV, according to the relation

$$\Delta V_e = \left(\beta_m/\beta + 1\right)\Delta V \quad (5)$$

For a given fracture strength of the crust and hence a given change in volume of the chamber ΔV the volume erupted, ΔV_e, increases with the volatile content of the magma, since the very large compressibility of the exsolved volatile phase can accommodate large changes in volume for relatively small changes in pressure. This leads to much larger erupted volumes for volatile-rich magmas (Bower and Woods, 1998; Huppert and Woods, 2002).

If an eruption is modelled with a simple frictional law associated with the frictional resistance in the conduit, fL, and the overpressure in the chamber, $\Delta P(t)$, which implicitly requires that the volatiles separate from the melt (i.e. perfect open system degassing with no gas remaining in the melt) as the magma ascends to the surface (Jaupart and Allègre, 1991; Menand and Phillips, 2007; Woods and Koyaguchi, 1994), then the mass flow rate is given by

$$dM/dt = \Delta P(t)/fL \qquad (6)$$

Combining this relation with equation (3), it follows that the eruption rate will decay exponentially with time according to the relation (Huppert and Woods, 2002)

$$dM/dt = \Delta P_C \exp\left(-fLt/M(\beta+\beta_m)\right) \qquad (7)$$

assuming constant coefficients for the frictional resistance. Since typical fracture pressures are of order 10^6 - 10^7 Pa (Touloukian et al., 1989), while the bulk compressibility is typically of order 10^{-8} – 10^{-10} Pa^{-1} for volatile-saturated and unsaturated magma, the volume of melt which erupts in such conduit or dyke-controlled eruptions may range from a few percent of the total volume of the chamber to a fraction of a percent in volatile-poor magmas. Equation 7 illustrates that the eruption duration increases with the compressibility of the magma, with the eruption duration t scaling as

$$t = M(\beta+\beta_m)/fL \qquad (8)$$

and this is consistent with the increased mass erupted for a volatile-saturated magma. The eruption rate depends primarily on $\Delta P(t)/fL$ as indicated by equation 6.

This model of the overall long-term control on eruption evolution, although simplified, can be compared with a number of historical eruption episodes for which the erupted volume has been

458 measured as a function of time, including the eruptions of Soufrière, St Vincent (Huppert et al.,
459 1982) and Paracutin, Mexico (Fries Jr, 1953), where the eruption rate seems to follow an
460 exponential decay law with time (**figure 6a**; after (Berkowitz and Woods, 2018 under review)).
461 However, there is growing evidence that in some some systems, there are multiple magma
462 reservoirs which can drive an eruption, and in particular, there is evidence that the eruption of
463 Eyjafyallojokull in 2010 involved mobilization of magma from three different levels in the crust,
464 in sequence, with a shallower magma reservoir being tapped, followed by an intermediate and
465 then a deep magma reservoir (Tarasewicz et al., 2012). This interpretation of multiple reservoirs
466 is also consistent with the eruption of Lonquimay (Moreno and Gardeweg, 1989) in which the
467 eruption rate showed a more complex evolution, with an initially rapid exponential decay during
468 the eruption of the first 50% of the magma, followed by a more gradual exponential decay during
469 the second phase of eruption (**figure 6b**). This eruption rate trend perhaps indicates a two
470 reservoir system, both of comparable size, in which the shallow reservoir initially erupts and
471 decompresses. This is then followed by the onset of eruption from the deeper reservoir, driving
472 new magma into the shallow reservoir, and causing the eruption to persist until the two reservoirs
473 re-equilibrate. In this case, one can envisage a double reservoir model, with a rate constant for
474 flow from the shallow reservoir to the surface, and a second rate constant for the flow between
475 the deeper and shallower reservoir (Berkowitz and Woods, 2018 under review).

476

477 Other historical eruptions also suggest that the gradual decompression of a deep magma reservoir
478 exerts a long term control on the eruption rate. For example, the 1980-1985 eruption of Mt St
479 Helens involved a series of intermittent slow dome-building and short dome-explosion events
480 following the initial major eruption episode (Brantley and Myers, 2000). Analysis of reported
481 data on the eruption volume during this 5-6 year period suggests a slow exponential decay of the
482 time-averaged eruption rate (**figure 6c**). Although the actual eruption history was intermittent,
483 owing to the non-linear controls associated with the formation and failure of the dome (Barmin et
484 al., 2002; Melnik and Sparks, 1999), the long term build up of pressure in the dome, between
485 each event appears to have been controlled by the flux from a gradually waning deeper reservoir
486 (Berkowitz and Woods, 2018 under review). Indeed, by modelling the non-linear valve-like
487 dynamics of the conduit feeding the dome in terms of a small critical overpressure for failure and
488 eruption of a shallow reservoir, the control on the long-term behavior of the system can be
489 rationalised in terms of the decompression of a deep reservoir.

490

491 **4. The role of the exsolved volatile phase in magma mixing and mingling**

Exsolved volatiles play an important role in magma mixing and mingling in magma reservoirs (Bachmann and Bergantz, 2006; Degruyter and Huber, 2014; Edmonds et al., 2010; Huber et al., 2011; Huppert and Woods, 2002; Pallister et al., 1996; Phillips and Woods, 2002; Ruprecht and Bachmann, 2010; Woods and Cowan, 2009). Magma intrusion has often been cited as a trigger for eruption (Eichelberger, 1980; Martin et al., 2008; Pallister et al., 1992; Sparks et al., 1977), and there is frequently petrological and geochemical evidence of magma mixing and /or heating shortly before eruptions (Metrich et al., 1993; Murphy et al., 2000; Rae et al., 2016; Ruprecht et al., 2012). Magma mingling may manifest as mafic inclusions and banded and streaked eruption products (Coombs et al., 2000; Plail et al., 2018; Sparks et al., 1977; Steiner et al., 2012; Tepley et al., 1999; Watts et al., 1999); and magma mixing as hybrid magmas, formed by the efficient mixing of magmas prior to eruption (which may encompass the disaggregation and scavenging of crystal phases), commonly displaying disequilibium textures and petrological features (Cassidy et al., 2015; Sparks and Marshall, 1986; Wright and Fiske, 1971). In this section we explore some general mechanisms, explored through analogue experiments and simple analytical models, by which the exsolved volatile phase may play a role in such processes, whereby intruding magma may interact with overlying magma, triggering mixing and eruption.

4.1. Magma mixing and overturn, driven by vesiculation of underplating basalt

If an intrusion of hot, relatively dense magma occurs below an existing body of cooled, evolved melt, the new lower layer of magma may inflate through cooling, crystallisation and exsolution of volatiles, but may remain dense relative to the overlying layer. It is possible, however, for this underplating magma to drive the eruption of the overlying magma (Burgisser and Bergantz, 2011; Huppert et al., 1982; Martin et al., 2008; Murphy et al., 2000; Sparks et al., 1984). The control on the erupted volume will be associated with the expansion of the volatiles in the underplating melt body, even though it is the overlying magma which erupts. The mass of magma erupted depends on the relative volume of the upper and lower layers of magma, since both will expand as the chamber pressure falls. With the upper layer erupting, the volume erupted as the pressure falls by an amount ΔP is now given by

$$\Delta V = \left(V_L \beta_L + V_u \beta_u + V\beta\right)\Delta P \qquad (9)$$

where $V_L + V_u = V$, the total magma reservoir volume. It follows that as the fractional volume change of the new volatile-rich magma (V_L) increases, the mass erupted also increases, even if

523 this is the less dense, overlying, degassed magma (V_u). This is because the mass erupted is
524 creating space for the expansion of the volatile-rich magma which is much more compressible
525 than the overlying magma.
526
527 The reduction in the density of the underplating body of magma, caused by cooling and
528 crystallization and associated exsolution of volatiles, may eventually cause this magma to
529 become less dense than the original magma in the reservoir. As a result, there may be an overturn
530 or mixing event, driven by degassing (Huppert et al., 1982; Ruprecht et al., 2008; Sparks et al.,
531 1984; Woods and Cowan, 2009). If the new, initially dense intrusion is relatively thin and of low
532 viscosity compared to the original melt, then the plumes of this low viscosity melt will be thin
533 and may become stirred into the overlying melt, especially if that melt is convecting. This can
534 lead to formation of mafic inclusions or an intermingled melt (Phillips and Woods, 2002). In
535 contrast, with a deeper or more viscous underplating magma, there may be a more complete
536 overturn, with plumes of the underplating magma being larger and accumulating at the top of the
537 overlying magma. In this case, on eruption, the crystalline mafic magma may be the dominant
538 phase which issues from the system. The intermingling, or mixing, produced by pre-eruption
539 cooling and crystallization has been explored in a series of experiments in which an increasing
540 volume of bubbles were created by electrolysis in a layer of viscous saline solution overlain by a
541 less dense, viscous bubble-free solution (**figure 7**) (Woods and Cowan, 2009). The experiments
542 illustrate the important control of the viscosity contrast between the melts as well as the relative
543 depths of the magma layers on whether there is stirring and mixing or overturn.
544
545 It is also possible that, during an eruption, the reduction in the pressure in the magma chamber
546 can lead to a reversal in the relative density of the two magmas (Ruprecht et al., 2008; Woods
547 and Cowan, 2009). This may lead to a change in the composition of the erupting magma during
548 the eruption provided that the eruption is sufficiently long-lived for overturn to occur. This
549 mechanism may provide an explanation for the heterogeneous chemical and textural
550 characteristics of crystal cargoes erupted in hybrid magmas, which suggest complex magmatic
551 mixing histories (Davidson and Tepley, 1997; Ruprecht et al., 2008; Singer et al., 1995). With a
552 typical density contrast of order 10-100 kg/m^3, magma of viscosity 100-1000 Pas and of depth
553 10-100 m, the time scale for overturn would be of order 10^3-10^4 s and this requires the eruption to
554 persist for a time of order hours, as is the case in larger explosive eruptions.
555

556 Woods and Cowan (2009) carried out a series of analogue experiments in which a volatile-rich
557 layer of saline and viscous natrasol solution underlay a volatile poor layer of relatively fresh but
558 viscous natrasol solution. The volatile phase was CO_2 dissolved in tap water. As the pressure is
559 reduced to pressures of order 0.01-0.1 of atmospheric pressure, the volatiles exsolve, and, in the
560 viscous solution, they form a bubble-rich layer. In the experiment, the upper solution was
561 generated from previously decompressed water in order to remove the volatiles prior the
562 experiment, and the salt added to the lower layer produced an initially density-stratified system.
563 As the system decompresses and the lower layer becomes less dense, the layers overturned. In a
564 further, unpublished experiment, an enclosed two layer system was connected to an upper tank
565 through two conduits providing a pathway for each of the layers to vent from the chamber, one
566 from the lower and one from the upper layer of system. The whole system was then enclosed in
567 sealed tank connected to the vacuum pump, Initially, as the system reached the pressure at which
568 some volatiles were exsolved from the lower layer, this layer expanded and an eruption began,
569 with the dense volatile-rich lower layer erupting through the lower conduit (right hand conduit,
570 figure 7) and the less dense volatile-poor solution erupting from the upper conduit (left hand
571 conduit, figure 7). However, as the experiment persisted and more volatiles were produced in the
572 lower layer, the density of the lower layer fell below that of the upper layer, and there was a
573 short-lived overturn event in the experimental tank. At this stage, the solution erupting from the
574 two conduits switched, as shown in the last panel in **figure 8**. The withdrawal of a lower viscosity
575 lower magma through an upper more viscous layer during eruption was also considered by
576 (Blake and Ivey, 1986).
577
578 4.2. *Vesiculation of underplating magmas and formation of mafic enclaves*
579 In the above discussion we have assumed that there is no separation of the bubbles from the melt-
580 crystal-bubble mixture, and that the melt-crystal mixture behaves as if it is a single fluid phase.
581 This leads to the idealised bulk flow behaviour described above. Although this is a powerful end-
582 member picture of the possible controls on overturn and eruption, the possible separation of the
583 volatile phase from the melt may influence such mixing processes and also the evolution of an
584 eruption and the eruption products and we now explore such effects, considering the impact of
585 bubble separation from a crystal-poor melt (Bottinga and Javoy, 1991; Jaupart and Vergniolle,
586 1989; Menand and Phillips, 2007; Woods and Cardoso, 1997).
587
588 In a low crystallinity melt, gas bubbles may rise. There are two modes of separation. First, the
589 bubbles can rise individually, following Stokes law, or a modified Stokes law including effects of

hindered ascent. Typically, for the bubbles that exist in magma reservoirs in the crust, this leads to rather slow rise speeds of order 10^{-10} – 10^{-6} m/s, depending on the bubble size and the melt viscosity. In addition to the ascent of individual bubbles, the presence of bubbles can lead to a convective flow, in which variations in the concentration of the bubbles through the melt lead to density differences and convective mixing of the melt (Cardoso and Woods, 1999). Cardoso and Woods (1997) showed, through experiment that this latter process stirs the melt and bubbles, but also leads to separation of the bubbles from the melt in the upper boundary layer of the flow through bubble-liquid slip.

In comparing the two processes, the ratio of the idealized Stokes speed of a bubble of size b and a parcel of fluid of size B with excess bubble concentration Δc relative to the surrounding melt is given by

$$V_b / V_B = b^2 / B^2 \Delta c \qquad (10)$$

where the Stokes speed is given by $V_b = 2\Delta\rho g b^2 / 9\mu$. Since the bubbles have typical sizes of order b = 0.1-1.0 mm in the chamber, the bubble rise speed is quite small, of order 10^{-10} – 10^{-6} m/s in magma with viscosity of order 10^2 – 10^4 Pa s, and so if there are small fluctuations in the concentration of bubbles through the melt layer, for example of magnitude Δc = 0.0001-0.01, the convective rise speed of parcels of bubble-rich melt will exceed the individual bubble rise speed provided the length scale of the parcel, B is greater than (10-100) b ~ 0.1-10 cm. If there are concentration fluctuations over greater length scales, as is very likely in a magma reservoir of scale 0.1 to 1.0 km, then convective mixing may dominate the individual rise of bubbles through the melt. Although convective mixing will tend to stir the bubbles throughout the melt, leading to a reasonably well-mixed suspension, near the top of the melt layer bubbles may separate from the melt and become trapped in a viscous boundary layer. The time scale for loss of bubbles from the main body of melt into this boundary layer scales with H / V_b, where H is the depth of the magma layer (Cardoso and Woods, 1999; Thomas et al., 1993; Woods and Cardoso, 1997). As a result, in either the case of individual bubble ascent or convective separation, the bubble-melt separation occurs over times which scale as H / V_b. With bubbles of size 0.1-1.0 mm in a magma of viscosity 10^2-10^4 Pas, the time to separate from a 100 m thick layer of melt is therefore in the range 10^8 – 10^{12} s. We infer that, with small bubbles in the more viscous melt, the time for separation may be relatively long (30,000 years) compared to the time scale of cooling and crystallisation of the

melt. In this case, cooling and crystallization will lead to further exsolution of volatiles and a build up of the chamber pressure which will tend to trigger an eruption of the bubble-laden melt. In addition, the accumulation of bubbles in the lower layer of melt will lower the density of this layer and tend to promote mixing or overturn of the magmas.

In contrast, for larger bubbles or a less viscous melt, bubble separation may occur within years, and so may be a dominant process inhibiting the tendency for large-scale overturn of the magma reservoir. Indeed with more primitive magmas, which have a low viscosity, bubble-melt separation can lead to bubble accumulation at the top of the magma body and the formation of a foam or bubble-rich layer. This is a mechanism proposed to be important for volatile exsolution in basaltic sills in the upper crust (Menand and Phillips, 2007), and in shallow reservoirs e.g., at Kilauea Volcano (Edmonds and Gerlach, 2007). If the system is closed, then the pressure will increase by a similar amount to that shown in the calculation above (*section 3.2*), in which the volatiles in the reservoir are assumed to remain well-mixed. However, in a reservoir of significant vertical extent there may be a significant additional pressurisation associated with the migration of the bubbles to the top of the chamber and the associated decrease in magmastatic pressure experienced by the bubbles. For example, in a chamber of order 1 km in vertical extent, bubble separation may lead to an additional overpressure of up to 1-10 MPa, but the effect is smaller in chambers of smaller vertical extent (Woods and Cardoso, 1997). If the magma has 0.5-1.0 wt% CO_2 and <0.5 wt% H_2O, and the reservoir is deeper than 2 km, the exsolved volatile phase will be enriched in CO_2 relative to H_2O. Leakage of this exsolved volatile phase from the roof zone of the magma reservoir may cause broad regions of diffuse CO_2 degassing inside calderas, as is observed at Kīlauea Volcano, Hawai‘i (Gerlach et al., 2002) and at many other active volcanoes exhibiting diffuse degassing between and during eruptive episodes (Salazar et al., 2001; Viveiros et al., 2010).

In some cases, the separation of the volatiles from the melt may then lead to a more continuous ‘open’ style of degassing of the volcanic system, either through Strombolian-style gas bursts. This can serve to regulate the pressure in the chamber and may tend to suppress larger, explosive eruptions. It has been proposed that if a foam layer develops at the top of a chamber or layer of basaltic melt, liquid drainage through the foam can lead to merger of the bubbles in the foam, and formation of larger gas slugs which may be responsible for larger Strombolian gas burst type eruptions (Houghton and Gonnermann, 2008; Houghton et al., 2016; Jaupart and Vergniolle, 1988; Vergniolle and Jaupart, 1986).

In *section 4.1* we discussed the possibility of a large scale overturn of the system if bubbles are exsolved in the lower layer of melt and this layer of melt is sufficiently viscous to retain the majority of the bubbles until its density falls below that of the upper layer. However, in some systems, there will be partial separation of the gas phase from the lower layer of melt, as described above, and this can lead to accumulation of a foam at the interface between the two layers of melt, especially if the upper layer is more viscous. If a sufficient fraction of the bubbles separate from the lower layer of melt, it may remain denser than the upper layer, suppressing any large scale overturn, while the foam forming at the interface between the layers will typically be less dense than the overlying layer of melt, leading to convective instability and ascent of parcels of foam into the overlying layer of melt. The percolation of a hot exsolved volatile phase from a mafic underplating layer upward into cooler, crystal-rich magma body has been proposed as a mechanism by which cool near-solidus magmas may 'defrost', triggering eruption (Bachmann and Bergantz, 2006; Huber et al., 2011; Huber et al., 2010). The exsolved volatile phase may also carry some of the mafic melt into the upper layer, leading to the formation of mafic inclusions in the upper layer (Andrews and Manga, 2014; Bacon, 1986; Eichelberger, 1980; Plail et al., 2014). These may eventually erupt if the overall pressure of the system becomes sufficient to trigger eruption of the upper layer (Phillips and Woods, 2002; Thomas et al., 1993). Good evidence for the accumulation of a foam layer at the interface between underplating basalts and overlying crystal-rich andesite comes from the observation, from enclaves erupted in Soufrière Hills Volcano andesite, that the enclaves are enriched in magnetite, interpreted to be due to the nucleation of aqueous fluid bubbles onto magnetite, which then "floated" up to the interface (Edmonds et al., 2014a).

Recently, it has been found that some mafic (basalt to basaltic andesite) inclusions (hosted in crystal-rich andesites at Soufrière Hills Volcano, Montserrat) are themselves composed of a mixture of the upper and lower melt (Plail et al., 2018), and this suggests that there is some mixing or intermingling of the magmas in either the foam layer or the lower layer prior to the formation of the mafic inclusions in the upper layer. This observation is common to many andesites containing mafic inclusions, such as the erupted products of Quizapu (Ruprecht et al., 2012) and Unzen, Japan (Browne et al., 2005). This intermingling of the magmas prior to formation of a mafic inclusion may arise if crystals in the upper layer become stirred into the lower layer. These are observed in the enclaves as plagioclase crystals with sieve textures and resorbed rims that have undergone heating after being mixed into more mafic melt (Humphreys

et al., 2009), which is a common feature of many mafic inclusions hosted by andesites and dacites (Leonard et al., 2002; Tepley et al., 1999). As the lower layer becomes progressively more crystalline and volatile-rich, a foamy layer may develop at the interface, carrying some of the hybrid interface magma up with the bubbles into the upper layer. Alternatively, when the mafic magma ponds below the existing layer of cooler and less dense melt, the heat transfer across the interface may lead to formation of a thin layer of relatively hot and mobile original magma and a corresponding thin layer of cooled, more crystalline and volatile-rich new magma which supplies the heat to the upper thin layer. Eventually, the lower cooled layer exsolves some volatiles, becomes less dense and intermingles with the heated boundary layer of original magma. This local overturn can produce intermingling and a hybrid layer of melt. As the heat transfer continues, the boundary layer becomes progressively deeper, enabling buoyant plumes from the intermingled boundary layer to rise into the upper, cooler layer of more viscous melt. As the boundary layer becomes deeper, mafic enclaves may become larger. In this multistage fashion, we can envisage that mafic inclusions of intermediate composition may be generated in the upper layer (Plail et al., 2018).

Whether wholescale overturn of magmas occurs, or whether gas-rich buoyant plumes (or even fractures, see next section) are generated from the interface between magmas, it seems clear that underplating basaltic magmas may supply significant quantities of exsolved volatiles to overlying magma reservoirs. Owing to the high sulfur content at sulfide saturation of basaltic melts (Jugo, 2009; Ripley and Li, 2013) it has been suggested that mafic underplating magmas may be an important source of the sulfur observed outgassing during volcanic eruptions via addition of sulfur-rich magmatic exsolved volatile phase to the overlying more evolved magma (Edmonds et al., 2010; Pallister et al., 1992; Roberge et al., 2009). Underplating mafic magmas, under some circumstances, may also play a role in generating more CO_2-rich magmatic vapor which may flux through shallower crystal-rich magmas (Blundy et al., 2010). The supply of volatiles from underplating mafic magmas has also been linked to the formation of copper porphyries. While crystal-rich, evolved magmas have capacity for producing the mass of copper required for a viable economic deposit, it has been suggested that additional sources of sulfur may be necessary, which may be supplied by mafic magmas intruding the evolved magma reservoir (Blundy et al., 2015; Hattori and Keith, 2001).

5. Exsolved volatile phase generation and transport through crystal-rich magma bodies

722 Magma bodies may spend much of their time in the crust near their solidus temperature, in a
723 partially or entirely crystalline state (Cashman et al., 2017; Cooper and Kent, 2014; Huber et al.,
724 2011; Huber et al., 2009; Huber et al., 2010; Koyaguchi and Kaneko, 1999; Marsh, 1981).
725 Volatile-rich basalts rising up into the crust will tend to underplate and interact with such
726 crystalline magma bodies (Bachmann and Bergantz, 2006; Edmonds et al., 2014b; Huber et al.,
727 2011), as discussed above. In this section we review and explore the range of behaviours possible
728 for storage and transport of the exsolved volatile phase in a crystal-rich mush and discuss the
729 implications for gas storage in and/or segregation from a mush, large syn-eruptive sulfur
730 emissions, ore deposits and the role of basaltic underplating in supplying volatiles to large, long-
731 lived crystalline magma bodies.
732
733 *5.1. Transport of an exsolved volatile phase in crystal-rich magma*
734 An underplating basalt will tend to pond and spread out beneath a cooler, less dense, more
735 evolved magma. The basalt will cool and crystallise against the cooler magma, generating a
736 buoyant volatile phase that may accumulate at the interface or rise upward, as described in
737 section *4*. The rate of volatile injection into the overlying crystal-rich magma depends on the
738 volatile content of the melt, the cooling rate and the convective motion of the underplating
739 magma (Cardoso and Woods, 1999; Huppert et al., 1982). The accumulation of an exsolved
740 volatile phase at the interface may cause a rheological instability, eventually leading to the foam
741 layer becoming buoyant and rising upward into the crystal-rich magma. It has been proposed that
742 the migration of this exsolved volatile phase into the overlying magma may remobilise the
743 crystal-rich magma due to the transfer of heat and partial melting (Bachmann and Bergantz,
744 2006; Huber et al., 2011; Huber et al., 2010). Reactivation and eruption of crystal-rich magmas
745 may be triggered in this way (Couch et al., 2001; Murphy et al., 2000; Pallister et al., 1992), with
746 the underplating basalt supplying volatiles which may be outgassed during the eruption
747 (Christopher et al., 2010; Edmonds et al., 2010).
748
749 As magma evolves and becomes progressively more crystalline, it is able to support a yield stress
750 and form a crystal framework (Caricchi et al., 2007; Lejeune and Richet, 1995; Pistone et al.,
751 2012) which tends to suppress the convective mixing or the ascent of bubbles. Such effects may
752 begin with crystal volume fractions of 0.2-0.3, depending on the shape and morphology of the
753 crystals, and as the crystal content increases, the yield stress increases (Pistone et al., 2012). In
754 addition, the viscosity of the crystalline mixture tends to be very much larger than the pure melt,
755 suppressing shear motions in the suspension. Recent experimental work has shown, however, that

the presence of hydrous fluid bubbles in a mush may have significant effects on its rheology. For mushes with crystal fractions of 0.55 to 0.7, for example, addition of volatiles such that bubble volume fractions of up to 0.1 are generated, leads to a dramatic reduction in viscosity by 3-4 orders of magnitude (Pistone et al., 2013). Furthermore, the viscosity of such three phase systems may be strain rate-dependent, with both shear thinning and shear thickening behaviour observed under different strain rates and crystal contents (Pistone et al., 2013).

As a result of this complex rheology, the process of gas separation from the crystal-rich magma takes on a range of forms. In a crystalline matrix, the migration process may be associated with either (a) gas flow through the porous matrix, which is likely to be a relatively slow process, owing to the low permeability of the formation (Parmigiani et al., 2016; Parmigiani et al., 2014) or (b) the generation of small effective fractures or cracks in the crystal-framework as the pressure exceeds the yield stress or effective fracture stress (Barth et al., in review; Huber et al., 2011). Such cracks then provide much higher permeability pathways through which an exsolved volatile phase may flow (Oppenheimer et al., 2015).

In more crystalline melts, these transport processes, which may be relatively rapid, may be responsible for the separation of the exsolved volatile phase from the melt and its accumulation at the roof zone, or in liquid-rich lenses in the magma reservoir system, where they may be held up (Parmigiani et al., 2016). These accumulations of exsolved volatiles may lead to large emissions of volcanic gases during eruptions. If the exsolved volatile phase at this pressure has a significant concentration of sulfur (Oppenheimer et al., 2011; Scaillet and Pichavant, 2003) then this mechanism of gas extraction may rationalise the high sulphur dioxide emissions from, for example, large explosive eruptions such as El Chichon (Mexico, 1982) (Bluth et al., 1997) and Pinatubo (Philippines, 1991) (Wallace and Gerlach, 1994). It is also likely that volcanoes which exhibit long-lived and persistent degassing, both during and between eruptions, may be tapping regions of crystal-rich magma reservoirs that have accumulated exsolved volatiles (Christopher et al., 2015; Edmonds et al., 2003).

In a series of experiments to model the *in situ* production of an exsolved volatile phase in a cooling and crystallising melt, a series of glass balls were placed in a tank filled with polymer-rich liquid and the mixture was gradually decompressed (Ptacek et al., 2018, sub judice). As the mixture reached the vapour-saturation pressure, volatiles gradually came out of solution and as the pressure was slowly decreased, the pack of beads gradually inflated. As this dilation occurred,

790 the effective permeability of the particle pack increased substantially and the gas was able to
791 migrate through the interstices between the glass beads, forming small gas channels in the matrix.
792 Once the gas escape rate exceeded the bubble generation rate, the expansion of the system was
793 arrested and indeed the gas-derived dilation reduced (panel 3, **figure 9**). In this way the gas was
794 able to separate from the melt-crystal mixture, and the pack relaxed back to a depth at which the
795 remaining gas phase was trapped as individual bubbles in the interstices between crystals, as may
796 be seen in panel 4 of **figure 9** (Ptacek et al., 2018, sub judice).
797
798 The processes controlling the rate of migration of gas through such a deformable permeable
799 matrix may involve both a regime of slow capillary gas flow through the permeable matrix
800 (Parmigiani et al., 2016) and a regime of more rapid gas flow following deformation of the pack
801 in which high permeability channels are created (Oppenheimer et al 2016). In the analogue
802 system of a clay-water mixture, the continued supply of gas to a clay-filled elastic reservoir may
803 lead to episodic pressurisation of the reservoir, followed by fracture of the clay seal, gas release
804 and build up of a further pressurisation cycle (Rocco et al., 2017). This process may be
805 analoguous to the intermittent gas-escape cycles which develop in a magmatic system as gas
806 pressure builds up and eventually exceeds the yield strength of the viscous-crystalline melt,
807 driving a pure gas channel through the particle-pack and allowing the system to decompress. A
808 similar phenomenon arises when gas is supplied from below to a close-packed mixture of
809 particles suspended in a high-viscosity liquid (Barth et al., in review). The gas tends to
810 accumulate in localised pockets within the deformable liquid-crystal pack. As the pressure builds
811 up, it is eventually able to generate a small fracture which provides a pathway through the
812 system, allowing the gas to continue rising through the formation, until the overpressure is
813 dissipated and the gas builds up a new pocket higher in the system.
814
815 These experiments of the migration of gas through a highly crystalline permeable matrix,
816 partially filled with melt, leads to a different mechanism of gas separation from underplating
817 basalts as the melt cools and crystallises. For a typical crystalline matrix, which is poorly
818 consolidated, the fracture strength or yielding strength may be of order 10^5-10^6 Pa (Saar et al.,
819 2001), which is smaller than the strength of a solid rock. As exsolved gases form and pressurize
820 the system they will therefore be able to open up fractures within the basalt along which they may
821 escape. We deduce that if a new intrusion of basalt cools and crystallises to the extent that it
822 becomes immobile or develops a yield stress while remaining denser than the overlying layer of

823 melt, then as volatiles are exsolved from this layer of melt, these volatiles can be transported via
824 fractures into the overlying original magma, as discussed by Huber et al., (2012).
825
826 A further phenomenon associated with gas migration through crystalline magmas is that, once the
827 main pulse of gas has passed through the magma, there will be a small fraction which is retained
828 in the pore spaces by capillary effects, and this will lead to the magma remaining in a more
829 compressible state than the pure volatile-free melt phase. Typically the residual saturation of gas
830 in a porous layer depends on the grain size and the interfacial tension between the solid minerals
831 and the melt phase. More experimental data is required to constrain these gas fractions, which
832 depend on the wetting angle of the gas and crystals relative to that of the melt and crystals.
833
834 The exsolved volatile phase may also play a role in magma differentiation and crystal-liquid
835 segregation in undercooled magmatic intrusions and in thin sheets of primitive magma
836 underplating cooler magma reservoirs: as the magma cools and crystallises, the buildup of gas
837 pressure due to second boiling may be relieved by expulsion of melt out of the region of
838 crystallization (Anderson Jr et al., 1984; Sisson and Bacon, 1999).
839
840 *5.2. Implications of our new understanding of the transport of the exsolved volatile phase*
841 *through crystalline magmas for ore deposits*
842 The exsolved magmatic volatile phase is understood to play a critical role in the formation of
843 porphyries which contain economic grades of metal deposits (Hedenquist and Lowenstern, 1994;
844 Lowenstern et al., 1991; Williams-Jones and Heinrich, 2005). Recent advances, discussed above,
845 in understanding how the exsolved volatile phase may be retained, and/or transported through
846 crystal-rich magma bodies have important implications for models of ore deposit formation and
847 for understanding why some magma reservoirs yield metal accumulations of economic
848 importance and others do not. As discussed in section *2*, magma may saturate in an exsolved
849 volatile phase during decompression, or during cooling and crystallization. Depending on the
850 initial H_2O and chlorine contents of the melt, and the pressure and temperature, a brine phase
851 may also form (Webster, 1997, Metrich and Rutherford, 1992, Webster, 1992, Shinohara, 1994).
852 The chlorinity of the exsolved volatile phase is critical for its metal-carrying capacity (Halter and
853 Webster, 2004). The exsolved volatile phase may migrate to the upper reaches of the magma
854 reservoir system through channelised flow through a crystal-rich magma, perhaps accumulating
855 in pockets before rising further up through the mush, as discussed in section *5*. Over time, the
856 lower density exsolved volatile phase will accumulate in the upper zones of the reservoir, or in

liquid lenses, where fracturing cannot occur (Parmigiani et al., 2016). This process of fluid migration through quasi-brittle fractures may be much faster than by bubble rise through permeable flow or through magma convection (Lowenstern, 1994; Shinohara et al., 1995). This therefore provides an efficient mechanism for segregation and accumulation of metals carried by saline, low density, exsolved fluids at the roof zones of mushy magma reservoirs (**figure 10**).

The "tonnage" of metals that may be accumulated in this way might then be expected to be proportional to the water content of the magma, which will determine the mass fraction of exsolved volatile phase, its chlorinity, which will depend on the chlorine content of the melt, temperature and pressure, the overall size of the magma reservoir and perhaps just as importantly, the crystallinity and structure of the reservoir. Extensive mush zones will allow rapid and efficient transport of metal-rich magmatic vapor to the roof zones of magma reservoirs, where excess pressure there will promote the intrusion of stocks and/or the triggering of volcanic eruptions.

For example, porphyries hosting molybdenum (Mo) deposits are formed from highly evolved, crystal-rich magmas, whereby Mo partitions from the silicate melt into a co-existing single fluid, at pressures above the critical point, with a fluid-melt partition coefficient of 5-20 (Audetat and Li, 2017; Zajacz et al., 2008). At lower pressures or temperatures, as the solidus is approached, this fluid may condense a brine phase. There is abundant evidence for extensive fluid transport at magmatic conditions: Mo mineralization commonly occurs only in the uppermost parts of vertically elongate magma bodies. The available data from a recent review of a number of Mo porphyries suggest that the parent magmas of such bodies were not particularly Mo-rich and the fluids from both mineralising and barren magma bodies are similar in terms of their geochemistry (Audétat and Li, 2017; Lowenstern, 1994), suggesting that instead, magma volume and depth, as well as the mechanism of volatile extraction from the mush, may be the most important factor. Previous workers have suggested magma convection and open system degassing as a mechanism for extracting the fluid phase from a large body of magma (Lowenstern, 1994; Shinohara et al., 1995). However, following recent work, as discussed above, on the mechanisms of porous flow and fracturing of crystal-rich magma, we now understand that fluid extraction from large-scale mush systems may take place efficiently on rapid timescales, thereby building accumulations of metals at the roof zones of large crystal-rich magma bodies (Huber et al., 2012).

6. Summary and problems for the future

In this review we have described some of the complex processes associated with the dynamical interactions of melt, crystals and volatiles. We show that most magmas, particularly those in subduction zone settings, are in equilibrium with an exsolved vapor phase through much of the evolution from the mid-crust to the surface and this exsolved volatile phase plays a fundamental role in magma differentiation, eruption triggering and the formation of hydrothermal ore deposits. We have distinguished between low crystal content, fluid-like systems in which the gas may drive convection in the melt, and higher crystal content, mushy systems, in which the gas may migrate by permeable flow or along fractures through the mush. We have also emphasized the role of exsolved volatiles in regulating the density and pressure of the magma and the chamber, with the exsolved volatile phase constraining the compressibility of the magma reservoir and the volume of melt erupted, given the change in volume of the magma chamber. Density changes in a stratified magma reservoir can lead to overturn or mixing and the formation of mafic inclusions especially in the case of fluid-like melt; whereas with a more crystalline system, density reversals may be less effective in that the convective overturn requires a buoyancy-derived stress to exceed the yield stress of the crystal-pack. However, if a series of fractures or channels open up to allow the exsolved volatiles to leak from the melt-crystal mixture, this can stabilise the vertical density profile of the magma reservoir over time. This mechanism of exsolved volatile phase migration to the apical zones of a magma reservoir over time can reconcile observations of large and/or persistent sulfur dioxide fluxes from volcanoes, as well as rapid timescales for the formation of hydrothermal ore deposits (e..g Cu porphyry-type deposits). Future work in this area might involve the use of volatile radionuclides at actively degassing volcanoes to establish the likely timescales of exsolved volatile accumulation in magma reservoirs.

There have been a series of key experiments measuring the shear stress in crystalline and crystal-bubble mixtures subjected to shear (Pistone et al., 2013), and some more recent experiments exploring the migration of gas through crystal-melt suspensions (Barth et al., in review; Oppenheimer et al., 2015; Ptacek et al., 2018, sub judice), but there is much more to learn about the macro-scale dynamics of the bulk fluid and how this interacts with the local dynamics of gas-melt separation, which can be facilitated through local deformation and fracture formation. Field observations of deformed bubbles and apparent shear bands in which melt is localized provide critical clues about the local processes of deformation and their relation to the large scale flow. Such observations suggest that there may also be critical effects associated with the varying compressibility of the magma as it ascends through the crust, and decompresses, perhaps leading to waves of volatile-rich and volatile-poor magma, connected by local shear bands or fractures.

The physical processes controlling crystal-rich magmas offers an area ripe for novel laboratory experiments, and these, combined with new field observations and careful geochemical analysis may be key in future efforts to unravel the history of co-erupted gas, melt and crystals.

Acknowledgements

We are grateful for support from the BP Institute, University of Cambridge.

References

Anderson, A.T., 1995. CO_2 and the eruptibility of picrite and komatiite. Lithos, 34(1–3): 19-25.

Anderson Jr, A.T., Swihart, G.H., Artioli, G. and Geiger, C.A., 1984. Segregation vesicles, gas filter-pressing, and igneous differentiation. The Journal of Geology, 92(1): 55-72.

Anderson, K. and Segall, P., 2011. Physics-based models of ground deformation and extrusion rate at effusively erupting volcanoes. Journal of Geophysical Research: Solid Earth, 116(B7).

Andrews, B.J. and Manga, M., 2014. Thermal and rheological controls on the formation of mafic enclaves or banded pumice. Contr. Mineral. and Petrol., 167(1): 961.

Atlas, Z.D., Dixon, J.E., Sen, G., Finny, M. and Martin-Del Pozzo, A.L., 2006. Melt inclusions from Volcán Popocatépetl and Volcán de Colima, Mexico: melt evolution due to vapor-saturated crystallization during ascent. Journal of Volcanology and Geothermal Research, 153(3-4): 221-240.

Audétat, A. and Li, W., 2017. The genesis of Climax-type porphyry Mo deposits: insights from fluid inclusions and melt inclusions. Ore Geology Reviews.

Bachmann, O. and Bergantz, G.W., 2006. Gas percolation in upper-crustal silicic crystal mushes as a mechanism for upward heat advection and rejuvenation of near-solidus magma bodies. Journal of Volcanology and Geothermal Research, 149(1): 85-102.

Bacon, C.R., 1986. Magmatic inclusions in silicic and intermediate volcanic rocks. Journal of Geophysical Research: Solid Earth, 91(B6): 6091-6112.

Bali, E., Hartley, M., Halldórsson, S., Gudfinnsson, G. and Jakobsson, S., 2018. Melt inclusion constraints on volatile systematics and degassing history of the 2014–2015 Holuhraun eruption, Iceland. Contr. Mineral. and Petrol., 173(2): 9.

Barclay, J., Carroll, M., Rutherford, M., Murphy, M., Devine, J., Gardner, J. and Sparks, R., 1998. Experimental phase equilibria constraints on pre-eruptive storage conditions of the Soufreiere Hills magma. Geophysical Research Letters(25): 3437-3440.

Barmin, A., Melnik, O. and Sparks, R., 2002. Periodic behavior in lava dome eruptions. Earth and Planetary Science Letters, 199(1-2): 173-184.

Barth, A., Edmonds, M. and Woods, A.W., in review. Valve-like dynamics of gas flow through a packed crystal mush and cyclic Strombolian explosions. Nature Communications.

Berkowitz and Woods, A., 2018 under review.

Berlo, K., Stix, J., Roggensack, K. and Ghaleb, B., 2012. A tale of two magmas, Fuego, Guatemala. Bull Volcanol, 74(2): 377-390.

Biggs, J. and Pritchard, M.E., 2017. Global volcano monitoring: what does it mean when volcanoes deform? Elements, 13(1): 17-22.

Blake, S., 1984. Volatile oversaturation during the evolution of silicic magma chambers as an eruption trigger. Journal of Geophysical Research: Solid Earth, 89(B10): 8237-8244.

971 Blake, S. and Ivey, G.N., 1986. Magma-mixing and the dynamics of withdrawal from stratified
972 reservoirs. Journal of Volcanology and Geothermal Research, 27(1-2): 153-178.
973 Blundy, J. and Cashman, K., 2005. Rapid decompression-driven crystallization recorded by melt
974 inclusions from Mount St. Helens volcano. Geology, 33(10): 793-796.
975 Blundy, J., Cashman, K.V., Rust, A. and Witham, F., 2010. A case for CO 2-rich arc magmas.
976 Earth and Planetary Science Letters, 290(3): 289-301.
977 Blundy, J., Mavrogenes, J., Tattitch, B., Sparks, S. and Gilmer, A., 2015. Generation of porphyry
978 copper deposits by gas-brine reaction in volcanic arcs. Nature Geoscience, 8(3): 235-240.
979 Bluth, G.J., Rose, W.I., Sprod, I.E. and Krueger, A.J., 1997. Stratospheric loading of sulfur from
980 explosive volcanic eruptions. The Journal of Geology, 105(6): 671-684.
981 Botcharnikov, R., Linnen, R. and Holtz, F., 2010. Solubility of Au in Cl-and S-bearing hydrous
982 silicate melts. Geochimica et Cosmochimica Acta, 74(8): 2396-2411.
983 Bottinga, Y. and Javoy, M., 1991. The degassing of Hawaiian tholeiite. Bull Volcanol, 53(2): 73-
984 85.
985 Bower, S.M. and Woods, A.W., 1998. On the influence of magma chambers in controlling the
986 evolution of explosive volcanic eruptions. Journal of Volcanology and Geothermal
987 Research, 86(1): 67-78.
988 Brantley, S. and Myers, B., 2000. Mount St. Helens-from the 1980 eruption to 2000. 2327-6932,
989 US Geological Survey.
990 Browne, B.L., Eichelberger, J.C., Patino, L.C., Vogel, T.A., Dehn, J., Uto, K. and Hoshizumi, H.,
991 2005. Generation of porphyritic and equigranular mafic enclaves during magma recharge
992 events at Unzen Volcano, Japan. Journal of Petrology, 47(2): 301-328.
993 Bucholz, C.E., Gaetani, G.A., Behn, M.D. and Shimizu, N., 2013. Post-entrapment modification
994 of volatiles and oxygen fugacity in olivine-hosted melt inclusions. Earth and Planetary
995 Science Letters.
996 Burgisser, A., Alletti, M. and Scaillet, B., 2015. Simulating the behavior of volatiles belonging to
997 the C–O–H–S system in silicate melts under magmatic conditions with the software D-
998 Compress. Computers & Geosciences, 79: 1-14.
999 Burgisser, A. and Bergantz, G.W., 2011. A rapid mechanism to remobilize and homogenize
1000 highly crystalline magma bodies. Nature, 471(7337): 212-215.
1001 Candela, P.A., 1997. A review of shallow, ore-related granites: textures, volatiles, and ore metals.
1002 Journal of petrology, 38(12): 1619-1633.
1003 Cardoso, S.S.S. and Woods, A.W., 1999. On convection in a volatile-saturated magma. Earth and
1004 Planetary Science Letters, 168(3–4): 301-310.
1005 Caricchi, L., Burlini, L., Ulmer, P., Gerya, T., Vassalli, M. and Papale, P., 2007. Non-Newtonian
1006 rheology of crystal-bearing magmas and implications for magma ascent dynamics. Earth
1007 and Planetary Science Letters, 264(3): 402-419.
1008 Caricchi, L., Sheldrake, T.E. and Blundy, J., 2018. Modulation of magmatic processes by CO 2
1009 flushing. Earth and Planetary Science Letters, 491: 160-171.
1010 Carn, S., Clarisse, L. and Prata, A., 2016. Multi-decadal satellite measurements of global
1011 volcanic degassing. Journal of Volcanology and Geothermal Research, 311: 99-134.
1012 Carroll, M. and Rutherford, M., 1985. Sulfide and sulfate saturation in hydrous silicate melts.
1013 Journal of Geophysical Research: Solid Earth (1978–2012), 90(S02): C601-C612.
1014 Cashman, K. and Blundy, J., 2000. Degassing and crystallization of ascending andesite and
1015 dacite. Philosophical Transactions of the Royal Society of London. Series A:
1016 Mathematical, Physical and Engineering Sciences, 358(1770): 1487-1513.
1017 Cashman, K. and Blundy, J., 2013. Petrological cannibalism: the chemical and textural
1018 consequences of incremental magma body growth. Contr. Mineral. and Petrol., 166(3):
1019 703-729.
1020 Cashman, K.V., 2004. Volatile controls on magma ascent and eruption. The State of the Planet:
1021 Frontiers and Challenges in Geophysics: 109-124.

1022 Cashman, K.V., Sparks, R.S.J. and Blundy, J.D., 2017. Vertically extensive and unstable
1023 magmatic systems: A unified view of igneous processes. Science, 355(6331): eaag3055.
1024 Cassidy, M., Edmonds, M., Watt, S.F., Palmer, M.R. and Gernon, T.M., 2015. Origin of Basalts
1025 by Hybridization in Andesite-dominated Arcs. Journal of Petrology: egv002.
1026 Chiaradia, M., Ulianov, A., Kouzmanov, K. and Beate, B., 2012. Why large porphyry Cu
1027 deposits like high Sr/Y magmas? Scientific reports, 2: 685.
1028 Chiodini, G., Caliro, S., De Martino, P., Avino, R. and Gherardi, F., 2012. Early signals of new
1029 volcanic unrest at Campi Flegrei caldera? Insights from geochemical data and physical
1030 simulations. Geology, 40(10): 943-946.
1031 Christopher, T., Blundy, J., Cashman, K., Cole, P., Edmonds, M., Smith, P., Sparks, R. and
1032 Stinton, A., 2015. Crustal-scale degassing due to magma system destabilization and
1033 magma-gas decoupling at Soufrière Hills Volcano, Montserrat. Geochemistry,
1034 Geophysics, Geosystems.
1035 Christopher, T., Edmonds, M., Humphreys, M. and Herd, R.A., 2010. Volcanic gas emissions
1036 from Soufrière Hills Volcano, Montserrat 1995–2009, with implications for mafic magma
1037 supply and degassing. Geophysical Research Letters, 37(19).
1038 Clémente, B., Scaillet, B. and Pichavant, M., 2004. The solubility of sulphur in hydrous rhyolitic
1039 melts. Journal of Petrology, 45(11): 2171-2196.
1040 Coombs, M.L., Eichelberger, J.C. and Rutherford, M.J., 2000. Magma storage and mixing
1041 conditions for the 1953–1974 eruptions of Southwest Trident volcano, Katmai National
1042 Park, Alaska. Contr. Mineral. and Petrol., 140(1): 99-118.
1043 Cooper, K.M. and Kent, A.J., 2014. Rapid remobilization of magmatic crystals kept in cold
1044 storage. Nature.
1045 Cordell, D., Unsworth, M.J. and Díaz, D., 2018. Imaging the Laguna del Maule Volcanic Field,
1046 central Chile using magnetotellurics: Evidence for crustal melt regions laterally-offset
1047 from surface vents and lava flows. Earth and Planetary Science Letters, 488: 168-180.
1048 Costa, F., Andreastuti, S., de Maisonneuve, C.B. and Pallister, J.S., 2013. Petrological insights
1049 into the storage conditions, and magmatic processes that yielded the centennial 2010
1050 Merapi explosive eruption. Journal of Volcanology and Geothermal Research, 261: 209-
1051 235.
1052 Couch, S., Sparks, R. and Carroll, M., 2001. Mineral disequilibrium in lavas explained by
1053 convective self-mixing in open magma chambers. Nature, 411(6841): 1037-1039.
1054 Davidson, J.P. and Tepley, F.J., 1997. Recharge in volcanic systems: evidence from isotope
1055 profiles of phenocrysts. Science, 275(5301): 826-829.
1056 De Maisonneuve, C.B., Dungan, M., Bachmann, O. and Burgisser, A., 2012. Insights into
1057 shallow magma storage and crystallization at Volcán Llaima (Andean Southern Volcanic
1058 Zone, Chile). Journal of Volcanology and Geothermal Research, 211: 76-91.
1059 Degruyter, W. and Huber, C., 2014. A model for eruption frequency of upper crustal silicic
1060 magma chambers. Earth and Planetary Science Letters, 403: 117-130.
1061 Dingwell, D., Romano, C. and Hess, K.-U., 1996. The effect of water on the viscosity of a
1062 haplogranitic melt under PTX conditions relevant to silicic volcanism. Contr. Mineral.
1063 and Petrol., 124(1): 19-28.
1064 Dingwell, D.B., 1996. Volcanic dilemma: flow or blow? Science, 273(5278): 1054.
1065 Dixon, J.E., Clague, D.A. and Stolper, E.M., 1991. Degassing history of water, sulfur, and carbon
1066 in submarine lavas from Kīlauea Volcano, Hawaii. The Journal of Geology: 371-394.
1067 Dixon, J.E. and Stolper, E.M., 1995. An experimental study of water and carbon dioxide
1068 solubilities in mid-ocean ridge basaltic liquids. Part II: applications to degassing. Journal
1069 of Petrology, 36(6): 1633-1646.
1070 Dixon, J.E., Stolper, E.M. and Holloway, J.R., 1995. An experimental study of water and carbon
1071 dioxide solubilities in mid-ocean ridge basaltic liquids. Part I: calibration and solubility
1072 models. Journal of Petrology, 36(6): 1607-1631.

1073 Edmonds, M., Aiuppa, A., Humphreys, M., Moretti, R., Giudice, G., Martin, R., Herd, R. and
1074 Christopher, T., 2010. Excess volatiles supplied by mingling of mafic magma at an
1075 andesite arc volcano. Geochemistry, Geophysics, Geosystems, 11(4).
1076 Edmonds, M., Brett, A., Herd, R., Humphreys, M. and Woods, A., 2014a. Magnetite-bubble
1077 aggregates at mixing interfaces in andesite magma bodies. Geological Society, London,
1078 Special Publications, 410: SP410. 417.
1079 Edmonds, M. and Gerlach, T.M., 2007. Vapor segregation and loss in basaltic melts. Geology,
1080 35(8): 751-754.
1081 Edmonds, M., Humphreys, M.C., Hauri, E.H., Herd, R.A., Wadge, G., Rawson, H., Ledden, R.,
1082 Plail, M., Barclay, J. and Aiuppa, A., 2014b. Pre-eruptive vapour and its role in
1083 controlling eruption style and longevity at Soufrière Hills Volcano. Geological Society,
1084 London, Memoirs, 39(1): 291-315.
1085 Edmonds, M., Kohn, S., Hauri, E., Humphreys, M. and Cassidy, M., 2016. Extensive, water-rich
1086 magma reservoir beneath southern Montserrat. Lithos, 252: 216-233.
1087 Edmonds, M., Oppenheimer, C., Pyle, D., Herd, R. and Thompson, G., 2003. SO 2 emissions
1088 from Soufrière Hills Volcano and their relationship to conduit permeability, hydrothermal
1089 interaction and degassing regime. Journal of Volcanology and Geothermal Research,
1090 124(1): 23-43.
1091 Edmonds, M., Pyle, D. and Oppenheimer, C., 2001. A model for degassing at the Soufrière Hills
1092 Volcano, Montserrat, West Indies, based on geochemical data. Earth and Planetary
1093 Science Letters, 186(2): 159-173.
1094 Eichelberger, J., 1980. Vesiculation of mafic magma during replenishment of silicic magma
1095 reservoirs. Nature, 288(5790): 446-450.
1096 Esposito, R., Hunter, J., Schiffbauer, J.D. and Bodnar, R.J., 2014. An assessment of the reliability
1097 of melt inclusions as recorders of the pre-eruptive volatile content of magmas. American
1098 Mineralogist, 99(5-6): 976-998.
1099 Fries Jr, C., 1953. Volumes and weights of pyroclastic material, lava, and water erupted by
1100 Paricutin volcano, Michoacan, Mexico. Eos, Transactions American Geophysical Union,
1101 34(4): 603-616.
1102 Gaetani, G.A., O'Leary, J.A., Shimizu, N., Bucholz, C.E. and Newville, M., 2012. Rapid
1103 reequilibration of H2O and oxygen fugacity in olivine-hosted melt inclusions. Geology,
1104 40(10): 915-918.
1105 Gerlach, T.M., 1980. Evaluation of volcanic gas analyses from Kīlauea volcano. Journal of
1106 Volcanology and Geothermal Research, 7(3–4): 295-317.
1107 Gerlach, T.M., McGee, K.A., Elias, T., Sutton, A.J. and Doukas, M.P., 2002. Carbon dioxide
1108 emission rate of Kīlauea Volcano: Implications for primary magma and the summit
1109 reservoir. Journal of Geophysical Research: Solid Earth, 107(B9): 2189.
1110 Ghiorso, M.S. and Gualda, G.A., 2015. An H2O–CO2 mixed fluid saturation model compatible
1111 with rhyolite-MELTS. Contr. Mineral. and Petrol., 169(6): 1-30.
1112 Grove, T., Parman, S., Bowring, S., Price, R. and Baker, M., 2002. The role of an H 2 O-rich
1113 fluid component in the generation of primitive basaltic andesites and andesites from the
1114 Mt. Shasta region, N California. Contr. Mineral. and Petrol., 142(4): 375-396.
1115 Guo, H. and Audétat, A., 2017. Transfer of volatiles and metals from mafic to felsic magmas in
1116 composite magma chambers: An experimental study. Geochimica et Cosmochimica Acta,
1117 198: 360-378.
1118 Halter, W.E. and Webster, J.D., 2004. The magmatic to hydrothermal transition and its bearing
1119 on ore-forming systems. Elsevier.
1120 Hartley, M.E., Maclennan, J., Edmonds, M. and Thordarson, T., 2014. Reconstructing the deep
1121 CO< sub> 2</sub> degassing behaviour of large basaltic fissure eruptions. Earth and
1122 Planetary Science Letters, 393: 120-131.

1123 Hartley, M.E., Neave, D.A., Maclennan, J., Edmonds, M. and Thordarson, T., 2015. Diffusive
1124 hydration of olivine-hosted melt inclusions. Earth and Planetary Science Letters, 425:
1125 168-178.
1126 Hattori, K.H. and Keith, J.D., 2001. Contribution of mafic melt to porphyry copper
1127 mineralization: evidence from Mount Pinatubo, Philippines, and Bingham Canyon, Utah,
1128 USA. Mineralium Deposita, 36(8): 799-806.
1129 Hautmann, S., Witham, F., Christopher, T., Cole, P., Linde, A.T., Sacks, I.S. and Sparks, R.S.J.,
1130 2014. Strain field analysis on Montserrat (WI) as tool for assessing permeable flow paths
1131 in the magmatic system of Soufrière Hills Volcano. Geochemistry, Geophysics,
1132 Geosystems, 15(3): 676-690.
1133 Hawkesworth, C., Blake, S., Evans, P., Hughes, R., Macdonald, R., Thomas, L., Turner, S. and
1134 Zellmer, G., 2000. Time scales of crystal fractionation in magma chambers—integrating
1135 physical, isotopic and geochemical perspectives. Journal of Petrology, 41(7): 991-1006.
1136 Hedenquist, J.W. and Lowenstern, J.B., 1994. The role of magmas in the formation of
1137 hydrothermal ore deposits. Nature, 370(6490): 519-527.
1138 Houghton, B. and Gonnermann, H., 2008. Basaltic explosive volcanism: constraints from
1139 deposits and models. Chemie der Erde-Geochemistry, 68(2): 117-140.
1140 Houghton, B., Taddeucci, J., Andronico, D., Gonnermann, H., Pistolesi, M., Patrick, M., Orr, T.,
1141 Swanson, D., Edmonds, M. and Gaudin, D., 2016. Stronger or longer: Discriminating
1142 between Hawaiian and Strombolian eruption styles. Geology, 44(2): 163-166.
1143 Huber, C., Bachmann, O. and Dufek, J., 2011. Thermo-mechanical reactivation of locked crystal
1144 mushes: Melting-induced internal fracturing and assimilation processes in magmas. Earth
1145 and Planetary Science Letters, 304(3): 443-454.
1146 Huber, C., Bachmann, O. and Manga, M., 2009. Homogenization processes in silicic magma
1147 chambers by stirring and mushification (latent heat buffering). Earth and Planetary
1148 Science Letters, 283(1): 38-47.
1149 Huber, C., Bachmann, O. and Manga, M., 2010. Two competing effects of volatiles on heat
1150 transfer in crystal-rich magmas: thermal insulation vs defrosting. Journal of Petrology,
1151 51(4): 847-867.
1152 Huber, C., Bachmann, O., Vigneresse, J.L., Dufek, J. and Parmigiani, A., 2012. A physical model
1153 for metal extraction and transport in shallow magmatic systems. Geochemistry,
1154 Geophysics, Geosystems, 13(8).
1155 Humphreys, M.C., Christopher, T. and Hards, V., 2009. Microlite transfer by disaggregation of
1156 mafic inclusions following magma mixing at Soufrière Hills volcano, Montserrat. Contr.
1157 Mineral. and Petrol., 157(5): 609-624.
1158 Huppert, H.E., Sparks, R.S.J. and Turner, J.S., 1982. Effects of volatiles on mixing in calc-
1159 alkaline magma systems. Nature, 297(5867): 554-557.
1160 Huppert, H.E. and Woods, A.W., 2002. The role of volatiles in magma chamber dynamics.
1161 Nature, 420(6915): 493-495.
1162 Jaupart, C. and Allègre, C.J., 1991. Gas content, eruption rate and instabilities of eruption regime
1163 in silicic volcanoes. Earth and Planetary Science Letters, 102(3-4): 413-429.
1164 Jaupart, C. and Vergniolle, S., 1988. Laboratory models of Hawaiian and Strombolian eruptions.
1165 Nature, 331(6151): 58-60.
1166 Jaupart, C. and Vergniolle, S., 1989. The generation and collapse of a foam layer at the roof of a
1167 basaltic magma chamber. Journal of Fluid Mechanics, 203: 347-380.
1168 Jugo, P.J., 2009. Sulfur content at sulfide saturation in oxidized magmas. Geology, 37(5): 415-
1169 418.
1170 Kent, A.J.R., 2008. Melt Inclusions in Basaltic and Related Volcanic Rocks. Reviews in
1171 Mineralogy and Geochemistry, 69(1): 273-331.
1172 Keppler, H., 1999. Experimental evidence for the source of excess sulfur in explosive volcanic
1173 eruptions. Science, 284(5420): 1652-1654.

1174 Kilbride, B.T.M., Mulina, K., Wadge, G., Johnson, R.W., Itikarai and Edmonds, M., 2018. Multi-
1175 year satellite observations of sulfur dioxide gas emissions and lava extrusion at
1176 Bagana volcano, Papua New Guinea. Frontiers in Earth Science.
1177 Kiser, E., Palomeras, I., Levander, A., Zelt, C., Harder, S., Schmandt, B., Hansen, S., Creager, K.
1178 and Ulberg, C., 2016. Magma reservoirs from the upper crust to the Moho inferred from
1179 high-resolution Vp and Vs models beneath Mount St. Helens, Washington State, USA.
1180 Geology, 44(6): 411-414.
1181 Koleszar, A.M., Saal, A.E., Hauri, E.H., Nagle, A.N., Liang, Y. and Kurz, M.D., 2009. The
1182 volatile contents of the Galapagos plume; evidence for H2O and F open system behavior
1183 in melt inclusions. Earth and Planetary Science Letters, 287(3–4): 442-452.
1184 Koyaguchi, T. and Kaneko, K., 1999. A two-stage thermal evolution model of magmas in
1185 continental crust. Journal of Petrology, 40(2): 241-254.
1186 Kuritani, T., Yoshida, T., Kimura, J.-I., Hirahara, Y. and Takahashi, T., 2014. Water content of
1187 primitive low-K tholeiitic basalt magma from Iwate Volcano, NE Japan arc: implications
1188 for differentiation mechanism of frontal-arc basalt magmas. Mineralogy and Petrology,
1189 108(1): 1-11.
1190 Lange, R.A., Frey, H.M. and Hector, J., 2009. A thermodynamic model for the plagioclase-liquid
1191 hygrometer/thermometer. American Mineralogist, 94(4): 494-506.
1192 Lavigne, F., Degeai, J.-P., Komorowski, J.-C., Guillet, S., Robert, V., Lahitte, P., Oppenheimer,
1193 C., Stoffel, M., Vidal, C.M. and Pratomo, I., 2013. Source of the great AD 1257 mystery
1194 eruption unveiled, Samalas volcano, Rinjani Volcanic Complex, Indonesia. Proceedings
1195 of the National Academy of Sciences, 110(42): 16742-16747.
1196 Lejeune, A.M. and Richet, P., 1995. Rheology of crystal-bearing silicate melts: An experimental
1197 study at high viscosities. Journal of Geophysical Research: Solid Earth, 100(B3): 4215-
1198 4229.
1199 Leonard, G., Cole, J., Nairn, I. and Self, S., 2002. Basalt triggering of the c. AD 1305 Kaharoa
1200 rhyolite eruption, Tarawera volcanic complex, New Zealand. Journal of Volcanology and
1201 Geothermal Research, 115(3): 461-486.
1202 Liu, Y., Anderson, A.T., Wilson, C.J., Davis, A.M. and Steele, I.M., 2006. Mixing and
1203 differentiation in the Oruanui rhyolitic magma, Taupo, New Zealand: evidence from
1204 volatiles and trace elements in melt inclusions. Contr. Mineral. and Petrol., 151(1): 71-87.
1205 Lloyd, A.S., Ferriss, E., Ruprecht, P., Hauri, E.H., Jicha, B.R. and Plank, T., 2016. An
1206 assessment of clinopyroxene as a recorder of magmatic water and magma ascent rate.
1207 Journal of Petrology, 57(10): 1865-1886.
1208 Lloyd, A.S., Plank, T., Ruprecht, P., Hauri, E.H. and Rose, W., 2013. Volatile loss from melt
1209 inclusions in pyroclasts of differing sizes. Contr. Mineral. and Petrol., 165(1): 129-153.
1210 Longo, A., Vassalli, M., Papale, P. and Barsanti, M., 2006. Numerical simulation of convection
1211 and mixing in magma chambers replenished with CO2-rich magma. Geophysical
1212 Research Letters, 33(21): L21305.
1213 Longpré, M.-A., Stix, J., Klügel, A. and Shimizu, N., 2017. Mantle to surface degassing of
1214 carbon-and sulphur-rich alkaline magma at El Hierro, Canary Islands. Earth and Planetary
1215 Science Letters, 460: 268-280.
1216 Lowenstern, J.B., 1994. Dissolved volatile concentrations in an ore-forming magma. Geology,
1217 22(10): 893-896.
1218 Lowenstern, J.B., 1995. Applications of silicate-melt inclusions to the study of magmatic
1219 volatiles. Magmas, fluids, and ore deposits, 23: 71-99.
1220 Lowenstern, J.B., Bacon, C.R., Calk, L.C., Hervig, R.L. and Aines, R.D., 1994. Major-element,
1221 trace-element, and volatile concentrations in silicate melt inclusions from the tuff of Pine
1222 Grove, Wah Wah Mountains, Utah. 2331-1258, US Geological Survey.
1223 Lowenstern, J.B., Mahood, G.A., Rivers, M.L. and Sutton, S.R., 1991. Evidence for extreme
1224 partitioning of copper into a magmatic vapor phase. Science, 252(5011): 1405-1409.

Lowenstern, J.B. and Sinclair, W.D., 1996. Exsolved magmatic fluid and its role in the formation of comb-layered quartz at the Cretaceous Logtung W-Mo deposit, Yukon Territory, Canada. Transactions of the Royal Society of Edinburgh: Earth Sciences, 87: 303.
Lu, Y.-J., Loucks, R.R., Fiorentini, M.L., Yang, Z.-M. and Hou, Z.-Q., 2015. Fluid flux melting generated postcollisional high Sr/Y copper ore–forming water-rich magmas in Tibet. Geology, 43(7): 583-586.
Luhr, J.F., Carmichael, I.S. and Varekamp, J.C., 1984. The 1982 eruptions of El Chichón Volcano, Chiapas, Mexico: mineralogy and petrology of the anhydritebearing pumices. Journal of Volcanology and Geothermal Research, 23(1-2): 69-108.
Maclennan, J., 2017. Bubble formation and decrepitation control the CO2 content of olivine-hosted melt inclusions. Geochemistry, Geophysics, Geosystems, 18(2): 597-616.
Marsh, B., 1981. On the crystallinity, probability of occurrence, and rheology of lava and magma. Contr. Mineral. and Petrol., 78(1): 85-98.
Martin, V.M., Morgan, D.J., Jerram, D.A., Caddick, M.J., Prior, D.J. and Davidson, J.P., 2008. Bang! Month-scale eruption triggering at Santorini volcano. Science, 321(5893): 1178-1178.
Mason, E., Edmonds, M. and Turchyn, A.V., 2017. Remobilization of crustal carbon may dominate volcanic arc emissions. Science, 357(6348): 290-294.
McCormick Kilbride, B., Edmonds, M. and Biggs, J., 2016. Observing eruptions of gas-rich compressible magmas from space. Nature Communications, 7.
Melekhova, E., Blundy, J., Martin, R., Arculus, R. and Pichavant, M., 2017. Petrological and experimental evidence for differentiation of water-rich magmas beneath St. Kitts, Lesser Antilles. Contr. Mineral. and Petrol., 172(11-12): 98.
Melnik, O. and Sparks, R., 1999. Nonlinear dynamics of lava dome extrusion. Nature, 402(6757): 37.
Melnik, O. and Sparks, R., 2002. Dynamics of magma ascent and lava extrusion at Soufrière Hills Volcano, Montserrat. Geological Society, London, Memoirs, 21(1): 153-171.
Menand, T. and Phillips, J.C., 2007. Gas segregation in dykes and sills. Journal of Volcanology and Geothermal Research, 159(4): 393-408.
Métrich, N., Bertagnini, A. and Di Muro, A., 2009. Conditions of magma storage, degassing and ascent at Stromboli: new insights into the volcano plumbing system with inferences on the eruptive dynamics. Journal of Petrology, 51(3): 603-626.
Metrich, N. and Clocchiatti, R., 1996. Sulfur abundance and its speciation in oxidized alkaline melts. Geochimica et Cosmochimica Acta, 60(21): 4151-4160.
Metrich, N., Clocchiatti, R., Mosbah, M. and Chaussidon, M., 1993. The 1989–1990 activity of Etna magma mingling and ascent of H 2 O□ Cl□ S□ rich basaltic magma. Evidence from melt inclusions. Journal of volcanology and geothermal research, 59(1): 131-144.
Métrich, N. and Wallace, P.J., 2008. Volatile Abundances in Basaltic Magmas and Their Degassing Paths Tracked by Melt Inclusions. Reviews in Mineralogy and Geochemistry, 69(1): 363-402.
Moore, G. and Carmichael, I., 1998. The hydrous phase equilibria (to 3 kbar) of an andesite and basaltic andesite from western Mexico: constraints on water content and conditions of phenocryst growth. Contr. Mineral. and Petrol., 130(3-4): 304-319.
Moore, G., Vennemann, T. and Carmichael, I., 1998a. An empirical model for the solubility of H2O in magmas to 3 kilobars. American Mineralogist, 83(1): 36-42.
Moore, G., Vennemann, T. and Carmichael, I.S.E., 1998b. An empirical model for the solubility of H ₂ O in magmas to 3 kilobars. American Mineralogist, 83(1-2): 36-42.
Moore, L.R., Gazel, E., Tuohy, R., Lloyd, A.S., Esposito, R., Steele-MacInnis, M., Hauri, E.H., Wallace, P.J., Plank, T. and Bodnar, R.J., 2015. Special Collection: Glasses, Melts, and Fluids, as Tools for Understanding Volcanic Processes and Hazards. Bubbles matter: An

assessment of the contribution of vapor bubbles to melt inclusion volatile budgets. American Mineralogist, 100(4): 806-823.
Moreno, H. and Gardeweg, M.C., 1989. La erupción reciente en el complejo volcánico Lonquimay (Diciembre 1988), Andes del Sur. Andean Geology, 16(1): 93-117.
Moretti, R., Papale, P. and Ottonello, G., 2003. A model for the saturation of COHS fluids in silicate melts. Geological Society, London, Special Publications, 213(1): 81-101.
Murphy, M., Sparks, R., Barclay, J., Carroll, M. and Brewer, T., 2000. Remobilization of andesite magma by intrusion of mafic magma at the Soufriere Hills Volcano, Montserrat, West Indies. Journal of petrology, 41(1): 21-42.
Neave, D.A., Passmore, E., Maclennan, J., Fitton, G. and Thordarson, T., 2013. Crystal–melt relationships and the record of deep mixing and crystallization in the ad 1783 Laki Eruption, Iceland. Journal of Petrology: egt027.
Neave, D.A. and Putirka, K.D., 2017. A new clinopyroxene-liquid barometer, and implications for magma storage pressures under Icelandic rift zones. American Mineralogist, 102(4): 777-794.
Newman, S. and Lowenstern, J.B., 2002. VolatileCalc: a silicate melt–H2O–CO2 solution model written in Visual Basic for excel. Computers & Geosciences, 28(5): 597-604.
Oppenheimer, C., Scaillet, B. and Martin, R.S., 2011. Sulfur degassing from volcanoes: source conditions, surveillance, plume chemistry and earth system impacts. Reviews in mineralogy and geochemistry, 73(1): 363-421.
Oppenheimer, J., Rust, A., Cashman, K. and Sandnes, B., 2015. Gas migration regimes and outgassing in particle-rich suspensions. Front. Phys. 3: 60. doi: 10.3389/fphy.
Pallister, J.S., Hoblitt, R.P., Meeker, G.P., Knight, R.J. and Siems, D.F., 1996. Magma mixing at Mount Pinatubo: petrographic and chemical evidence from the 1991 deposits. Fire and mud: eruptions and lahars of Mount Pinatubo, Philippines: 687-731.
Pallister, J.S., Hoblitt, R.P. and Reyes, A.G., 1992. A basalt trigger for the 1991 eruptions of Pinatubo Volcano? Nature, 356(6368): 426.
Pan, V., Holloway, J.R. and Hervig, R.L., 1991. The pressure and temperature dependence of carbon dioxide solubility in tholeiitic basalt melts. Geochimica et Cosmochimica Acta, 55(6): 1587-1595.
Papale, P., 1999. Modeling of the solubility of a two-component H ₂ O+CO ₂ fluid in silicate liquids. American Mineralogist, 84(4): 477-492.
Parmigiani, A., Faroughi, S., Huber, C., Bachmann, O. and Su, Y., 2016. Bubble accumulation and its role in the evolution of magma reservoirs in the upper crust. Nature, 532(7600): 492-495.
Parmigiani, A., Huber, C. and Bachmann, O., 2014. Mush microphysics and the reactivation of crystal-rich magma reservoirs. Journal of Geophysical Research: Solid Earth, 119(8): 6308-6322.
Phillips, J.C. and Woods, A.W., 2002. Suppression of large-scale magma mixing by melt–volatile separation. Earth and Planetary Science Letters, 204(1): 47-60.
Pistone, M., Caricchi, L., Ulmer, P., Burlini, L., Ardia, P., Reusser, E., Marone, F. and Arbaret, L., 2012. Deformation experiments of bubble-and crystal-bearing magmas: Rheological and microstructural analysis. Journal of Geophysical Research: Solid Earth, 117(B5).
Pistone, M., Caricchi, L., Ulmer, P., Reusser, E. and Ardia, P., 2013. Rheology of volatile-bearing crystal mushes: mobilization vs. viscous death. Chemical Geology, 345: 16-39.
Plail, M., Barclay, J., Humphreys, M.C., Edmonds, M., Herd, R.A. and Christopher, T.E., 2014. Characterization of mafic enclaves in the erupted products of Soufrière Hills Volcano, Montserrat, 2009 to 2010. Geological Society, London, Memoirs, 39(1): 343-360.
Plail, M., Edmonds, M., Woods, A.W., Barclay, J., Humphreys, M.C., Herd, R.A. and Christopher, T., 2018. Mafic enclaves record syn-eruptive basalt intrusion and mixing. Earth and Planetary Science Letters, 484: 30-40.

1326 Plank, T., Kelley, K.A., Zimmer, M.M., Hauri, E.H. and Wallace, P.J., 2013. Why do mafic arc
1327 magmas contain~ 4wt% water on average? Earth and Planetary Science Letters, 364: 168-
1328 179.
1329 Pritchard, M.E. and Gregg, P.M., 2016. Geophysical evidence for silicic crustal melt in the
1330 continents: where, what kind, and how much? Elements, 12(2): 121-127.
1331 Prouteau, G. and Scaillet, B., 2003. Experimental constraints on the origin of the 1991 Pinatubo
1332 dacite. Journal of Petrology, 44(12): 2203-2241.
1333 Ptacek, M., Edmonds, M. and Woods, A., 2018, sub judice. TBA. J. .
1334 Putirka, K.D., 2005. Igneous thermometers and barometers based on plagioclase+ liquid
1335 equilibria: Tests of some existing models and new calibrations. American Mineralogist,
1336 90(2-3): 336-346.
1337 Rae, A., Edmonds, M., Morgan, D.J., Kahl, M., Houghton, B.F. and Maclennan, J., 2016.
1338 Timescales of magma mixing prior to and during the 1959 Kilauea Iki eruption. Geology
1339 44(6): 463-466.
1340 Richards, J.P., 2011. High Sr/Y arc magmas and porphyry Cu±Mo±Au deposits: just add water.
1341 Economic Geology, 106(7): 1075-1081.
1342 Ripley, E.M. and Li, C., 2013. Sulfide saturation in mafic magmas: is external sulfur required for
1343 magmatic Ni-Cu-(PGE) ore genesis? Economic Geology, 108(1): 45-58.
1344 Rivalta, E. and Segall, P., 2008. Magma compressibility and the missing source for some dike
1345 intrusions. Geophysical Research Letters, 35(4): L04306.
1346 Roberge, J., Delgado-Granados, H. and Wallace, P.J., 2009. Mafic magma recharge supplies high
1347 CO2 and SO2 gas fluxes from Popocatépetl volcano, Mexico. Geology, 37(2): 107-110.
1348 Robock, A., 2000. Volcanic eruptions and climate. Reviews of Geophysics, 38(2): 191-219.
1349 Rocco, S., Woods, A.W., Harrington, J. and Norris, S., 2017. An experimental model of episodic
1350 gas release through fracture of fluid confined within a pressurized elastic reservoir.
1351 Geophysical Research Letters, 44(2): 751-759.
1352 Roggensack, K., 2001. Unraveling the 1974 eruption of Fuego volcano (Guatemala) with small
1353 crystals and their young melt inclusions. Geology, 29(10): 911-914.
1354 Roggensack, K., Williams, S.N., Schaefer, S.J. and Parnell Jr, R.A., 1996. Volatiles from the
1355 1994 eruptions fo Rabaul: Understanding large caldera systems. Science, 273(5274): 490.
1356 Rose-Koga, E.F., Koga, K.T., Hamada, M., Hélouis, T., Whitehouse, M.J. and Shimizu, N., 2014.
1357 Volatile (F and Cl) concentrations in Iwate olivine-hosted melt inclusions indicating low-
1358 temperature subduction. Earth, Planets and Space, 66(1): 81.
1359 Ruprecht, P. and Bachmann, O., 2010. Pre-eruptive reheating during magma mixing at Quizapu
1360 volcano and the implications for the explosiveness of silicic arc volcanoes. Geology,
1361 38(10): 919-922.
1362 Ruprecht, P., Bergantz, G.W., Cooper, K.M. and Hildreth, W., 2012. The crustal magma storage
1363 system of Volcán Quizapu, Chile, and the effects of magma mixing on magma diversity.
1364 Journal of Petrology: egs002.
1365 Ruprecht, P., Bergantz, G.W. and Dufek, J., 2008. Modeling of gas-driven magmatic overturn:
1366 Tracking of phenocryst dispersal and gathering during magma mixing. Geochemistry,
1367 Geophysics, Geosystems, 9(7).
1368 Ruth, D.C., Cottrell, E., Cortés, J.A., Kelley, K.A. and Calder, E.S., 2016. From passive
1369 degassing to violent strombolian eruption: the case of the 2008 eruption of Llaima
1370 volcano, Chile. Journal of Petrology, 57(9): 1833-1864.
1371 Saar, M.O., Manga, M., Cashman, K.V. and Fremouw, S., 2001. Numerical models of the onset
1372 of yield strength in crystal–melt suspensions. Earth and Planetary Science Letters, 187(3):
1373 367-379.
1374 Saito, G., Kazahaya, K., Shinohara, H., Stimac, J. and Kawanabe, Y., 2001. Variation of volatile
1375 concentration in a magma system of Satsuma-Iwojima volcano deduced from melt
1376 inclusion analyses. Journal of Volcanology and Geothermal Research, 108(1-4): 11-31.

Salazar, J.M., Hernández, P.A., Pérez, N.M., Melián, G., Álvarez, J., Segura, F. and Notsu, K., 2001. Diffuse emission of carbon dioxide from Cerro Negro volcano, Nicaragua, Central America. Geophysical Research Letters, 28(22): 4275-4278.

Scaillet, B., Clémente, B., Evans, B.W. and Pichavant, M., 1998. Redox control of sulfur degassing in silicic magmas. Journal of Geophysical Research: Solid Earth (1978–2012), 103(B10): 23937-23949.

Scaillet, B. and Pichavant, M., 2003. Experimental constraints on volatile abundances in arc magmas and their implications for degassing processes. Geological Society, London, Special Publications, 213(1): 23-52.

Scaillet, B. and Pichavant, M., 2005. A model of sulphur solubility for hydrous mafic melts: application to the determination of magmatic fluid compositions of Italian volcanoes. Annals of Geophysics.

Segall, P., 2013. Volcano deformation and eruption forecasting. Geological Society, London, Special Publications, 380(1): 85-106.

Shinohara, H., Kazahaya, K. and Lowenstern, J.B., 1995. Volatile transport in a convecting magma column: Implications for porphyry Mo mineralization. Geology, 23(12): 1091-1094.

Sides, I., Edmonds, M., Maclennan, J., Houghton, B., Swanson, D. and Steele-MacInnis, M., 2014a. Magma mixing and high fountaining during the 1959 Kīlauea Iki eruption, Hawai ‘i. Earth and Planetary Science Letters, 400: 102-112.

Sides, I.R., Edmonds, M., Maclennan, J., Swanson, D.A. and Houghton, B.F., 2014b. Eruption style at Kīlauea Volcano in Hawai`i linked to primary melt composition Nature Geoscience, 7: 464–469.

Singer, B.S., Dungan, M.A. and Layne, G.D., 1995. Textures and Sr, Ba, Mg, Fe, K, and Ti compositional profiles in volcanic plagioclase: clues to the dynamics of calc-alkaline magma chambers. American Mineralogist, 80(7-8): 776-798.

Sisson, T. and Bacon, C., 1999. Gas-driven filter pressing in magmas. Geology, 27(7): 613-616.

Sisson, T. and Grove, T., 1993. Experimental investigations of the role of H2O in calc-alkaline differentiation and subduction zone magmatism. Contr. Mineral. and Petrol., 113(2): 143-166.

Sisson, T. and Layne, G., 1993. H2O in basalt and basaltic andesite glass inclusions from four subduction-related volcanoes. Earth and Planetary Science Letters, 117(3-4): 619-635.

Sparks, R., Huppert, H., Turner, J., Sakuyama, M. and O'Hara, M., 1984. The fluid dynamics of evolving magma chambers. Philosophical Transactions of the Royal Society of London A: Mathematical, Physical and Engineering Sciences, 310(1514): 511-534.

Sparks, R. and Marshall, L., 1986. Thermal and mechanical constraints on mixing between mafic and silicic magmas. Journal of Volcanology and Geothermal Research, 29(1-4): 99-124.

Sparks, S.R., Sigurdsson, H. and Wilson, L., 1977. Magma mixing: a mechanism for triggering acid explosive eruptions. Nature, 267(5609): 315-318.

Spilliaert, N., Allard, P., Métrich, N. and Sobolev, A., 2006. Melt inclusion record of the conditions of ascent, degassing, and extrusion of volatile-rich alkali basalt during the powerful 2002 flank eruption of Mount Etna (Italy). Journal of Geophysical Research: Solid Earth (1978–2012), 111(B4).

Steele-Macinnis, M., Esposito, R. and Bodnar, R.J., 2011. Thermodynamic model for the effect of post-entrapment crystallization on the H2O–CO2 systematics of vapor-saturated, silicate melt inclusions. Journal of Petrology, 52(12): 2461-2482.

Steiner, A.R., Browne, B.L. and Nye, C.J., 2012. Quenched mafic inclusions in≤ 2200 years BP deposits at Augustine Volcano, Alaska. International Geology Review, 54(11): 1241-1270.

1426 Stolper, E. and Holloway, J.R., 1988. Experimental determination of the solubility of carbon
1427 dioxide in molten basalt at low pressure. Earth and Planetary Science Letters, 87(4): 397-
1428 408.
1429 Symonds, R.B., Rose, W.I., Bluth, G.J. and Gerlach, T.M., 1994. Volcanic-gas studies; methods,
1430 results, and applications. Reviews in Mineralogy and Geochemistry, 30(1): 1-66.
1431 Tait, S., Jaupart, C. and Vergniolle, S., 1989. Pressure, gas content and eruption periodicity of a
1432 shallow, crystallising magma chamber. Earth and Planetary Science Letters, 92(1): 107-
1433 123.
1434 Tarasewicz, J., White, R.S., Woods, A.W., Brandsdóttir, B. and Gudmundsson, M.T., 2012.
1435 Magma mobilization by downward-propagating decompression of the Eyjafjallajökull
1436 volcanic plumbing system. Geophysical Research Letters, 39(19).
1437 Tepley, F., Davidson, J. and Clynne, M., 1999. Magmatic interactions as recorded in plagioclase
1438 phenocrysts of Chaos Crags, Lassen Volcanic Center, California. Journal of Petrology,
1439 40(5): 787-806.
1440 Thomas, N., Tait, S. and Koyaguchi, T., 1993. Mixing of stratified liquids by the motion of gas
1441 bubbles: application to magma mixing. Earth and Planetary Science Letters, 115(1-4):
1442 161-175.
1443 Touloukian, Y.S., W. R. Judd and Roy, R.F., 1989. Physical Properties of Rocks and Minerals
1444 McGraw-Hill, New York., 11(2).
1445 Ushioda, M., Takahashi, E., Hamada, M. and Suzuki, T., 2014. Water content in arc basaltic
1446 magma in the Northeast Japan and Izu arcs: an estimate from Ca/Na partitioning between
1447 plagioclase and melt. Earth, Planets and Space, 66(1): 127.
1448 Vergniolle, S. and Jaupart, C., 1986. Separated two-phase flow and basaltic eruptions. Journal of
1449 Geophysical Research: Solid Earth, 91(B12): 12842-12860.
1450 Vidal, C.M., Métrich, N., Komorowski, J.-C., Pratomo, I., Michel, A., Kartadinata, N., Robert, V.
1451 and Lavigne, F., 2016. The 1257 Samalas eruption (Lombok, Indonesia): the single
1452 greatest stratospheric gas release of the Common Era. Scientific Reports, 6: 34868.
1453 Viveiros, F., Cardellini, C., Ferreira, T., Caliro, S., Chiodini, G. and Silva, C., 2010. Soil CO2
1454 emissions at Furnas volcano, São Miguel Island, Azores archipelago: Volcano monitoring
1455 perspectives, geomorphologic studies, and land use planning application. Journal of
1456 Geophysical Research: Solid Earth (1978–2012), 115(B12).
1457 Voight, B., Widiwijayanti, C., Mattioli, G., Elsworth, D., Hidayat, D. and Strutt, M., 2010.
1458 Magma-sponge hypothesis and stratovolcanoes: Case for a compressible reservoir and
1459 quasi-steady deep influx at Soufrière Hills Volcano, Montserrat. Geophysical Research
1460 Letters, 37(19).
1461 Wallace, P., 2001. Volcanic SO 2 emissions and the abundance and distribution of exsolved gas
1462 in magma bodies. Journal of Volcanology and Geothermal Research, 108(1): 85-106.
1463 Wallace, P.J., 2005. Volatiles in subduction zone magmas: concentrations and fluxes based on
1464 melt inclusion and volcanic gas data. Journal of Volcanology and Geothermal Research,
1465 140(1): 217-240.
1466 Wallace, P.J., Anderson, A.T. and Davis, A.M., 1999. Gradients in H2O, CO2, and exsolved gas
1467 in a large-volume silicic magma system: Interpreting the record preserved in melt
1468 inclusions from the Bishop Tuff. Journal of Geophysical Research: Solid Earth, 104(B9):
1469 20097-20122.
1470 Wallace, P.J. and Edmonds, M., 2011. The sulfur budget in magmas: evidence from melt
1471 inclusions, submarine glasses, and volcanic gas emissions. Reviews in Mineralogy and
1472 Geochemistry, 73(1): 215-246.
1473 Wallace, P.J. and Gerlach, T.M., 1994. Magmatic vapor source for sulfur dioxide released during
1474 volcanic eruptions: evidence from Mount Pinatubo. Science, 265(5171): 497-499.

Wallace, P.J., Kamenetsky, V.S. and Cervantes, P., 2015. Melt inclusion CO2 contents, pressures of olivine crystallization, and the problem of shrinkage bubbles. American Mineralogist, 100(4): 787-794.
Waters, L.E. and Lange, R.A., 2015. An updated calibration of the plagioclase-liquid hygrometer-thermometer applicable to basalts through rhyolites. American Mineralogist, 100(10): 2172-2184.
Watts, R.B., de Silva, S.L., de Rios, G.J. and Croudace, I., 1999. Effusive eruption of viscous silicic magma triggered and driven by recharge: a case study of the Cerro Chascon-Runtu Jarita Dome Complex in Southwest Bolivia. Bull Volcanol, 61(4): 241-264.
Westrich, H. and Gerlach, T., 1992. Magmatic gas source for the stratospheric SO2 cloud from the June 15, 1991, eruption of Mount Pinatubo. Geology, 20(10): 867-870.
Williams-Jones, A.E. and Heinrich, C.A., 2005. 100th Anniversary special paper: vapor transport of metals and the formation of magmatic-hydrothermal ore deposits. Economic Geology, 100(7): 1287-1312.
Witham, F., Blundy, J., Kohn, S.C., Lesne, P., Dixon, J., Churakov, S.V. and Botcharnikov, R., 2012. SolEx: A model for mixed COHSCl-volatile solubilities and exsolved gas compositions in basalt. Computers & Geosciences, 45: 87-97.
Woods, A.W. and Cardoso, S.S., 1997. Triggering basaltic volcanic eruptions by bubble-melt separation. Nature, 385(6616): 518.
Woods, A.W. and Cowan, A., 2009. Magma mixing triggered during volcanic eruptions. Earth and Planetary Science Letters, 288(1): 132-137.
Woods, A.W. and Huppert, H.E., 2003. On magma chamber evolution during slow effusive eruptions. Journal of Geophysical Research: Solid Earth, 108(B8).
Woods, A.W. and Koyaguchi, T., 1994. Transitions between explosive and effusive eruptions of silicic magmas. Nature, 370(6491): 641-644.
Wright, T.L. and Fiske, R.S., 1971. Origin of the differentiated and hybrid lavas of Kilauea volcano, Hawaii. Journal of Petrology, 12(1): 1-65.
Zajacz, Z., Candela, P.A., Piccoli, P.M. and Sanchez-Valle, C., 2012. The partitioning of sulfur and chlorine between andesite melts and magmatic volatiles and the exchange coefficients of major cations. Geochimica et Cosmochimica Acta, 89: 81-101.
Zajacz, Z. and Halter, W., 2009. Copper transport by high temperature, sulfur-rich magmatic vapor: Evidence from silicate melt and vapor inclusions in a basaltic andesite from the Villarrica volcano (Chile). Earth and Planetary Science Letters, 282(1): 115-121.

Figure captions

Figure 1: Schematic diagram to illustrate how magmas may achieve volatile-saturation. A: decompressing silicate melt achieves saturation in an exsolved volatile phase, which promotes degassing-induced crystallisation. B: Isobaric crystallisation in a crustal magma reservoir causes second boiling and development of an exsolved volatile phase. MVP: (exsolved) magmatic volatile phase.

Figure 2: Solubility model for rhyolite (Newman and Lowenstern, 2002), showing melt CO_2 concentration versus melt water concentration. Isobars are in black solid lines, and represent the

1520 locus of values for dissolved H_2O and CO_2 in rhyolitic melt in equilibrium with H_2O–CO_2 vapor
1521 at 800C and selected pressures (labelled, in MPa). Isopleths are dashed lines, and represent the
1522 locus of rhyolitic melt compositions in equilibrium with the given exsolved volatile phase
1523 compositions: 20 mol% H_2O (80 mol% CO_2), 50 mol% H_2O and CO_2; and 80 mol% H_2O (20
1524 mol% CO_2) at 800 C. The orange and red dots show the behaviour of vapour-undersaturated and
1525 vapor-saturated melts (respectively) with (top orange dot) and without (bottom orange dot) CO_2.
1526 These examples are discussed in the text.
1527
1528 **Figure 3**: Evolution of melt H_2O content (red, in wt%) and total fraction of exsolved water (blue,
1529 in wt%) during crystallization from basalt to rhyolite, at 200 MPa, illustrating how substantial
1530 fractions of exsolved volatiles may be generated during isobaric crystallization. Curves are
1531 labelled with the initial basalt melt H_2O content, in wt%. If the evolved liquids and exsolved
1532 volatiles are segregated from their crystalline products, the fraction of exsolved volatiles in the
1533 magma (melt) is much higher than shown. For magma crystallization at lower and higher
1534 pressures, fractions of exsolved volatiles reach higher and lower values respectively (due to the
1535 lower and higher solubilities of water, respectively). Calculations are made using RhyoliteMelts
1536 (Ghiorso and Gualda, 2015).
1537
1538 **Figure 4:** Melt inclusion CO_2 and H_2O concentrations; and isobars to show volatile
1539 concentrations in equilibrium with an exsolved volatile phase for different pressures (marked). A:
1540 Volatile data for basaltic melt inclusions, hosted by olivine. Isobars are appropriate for Canary
1541 Island basalt (Burgisser et al., 2015). Data are shown for Fernandina and Santiago from (Koleszar
1542 et al., 2009); for Kīlauea from (Sides et al., 2014b), for El Hierro from (Longpré et al., 2017) for
1543 Laki (Hartley et al., 2014) , for Holuhraun (Bali et al., 2018), for Stromboli (Métrich et al., 2009),
1544 for Etna (Spilliaert et al., 2006) for Llaima (De Maisonneuve et al., 2012; Ruth et al., 2016) and
1545 for Fuego (Berlo et al., 2012; Lloyd et al., 2016; Roggensack, 2001; Sisson and Layne, 1993). B:
1546 Data for dacitic and rhyolitic melt inclusions, hosted by plagioclase and quartz. Isobars
1547 appropriate for rhyolite (Newman and Lowenstern, 2002). Data are shown for Pine Grove
1548 (Lowenstern et al., 1994), Soufrière Hills (Edmonds et al., 2014b), Bishop Tuff (Wallace et al.,
1549 1999), Oruanui, Taupo (Liu et al., 2006), Rabaul (Roggensack et al., 1996), Popocatepetl (Atlas
1550 et al., 2006) and Satsuma-Iwojima (Saito et al., 2001).
1551
1552 **Figure 5**. The effects of an exsolved volatile phase on magma compressibility and how it may
1553 evolve during magma fractionation in a magma reservoir. A) Effective compressibility of a melt-

1554 volatile mixture (with no crystals) in the case that there is 2, 4 and 6 wt% H_2O in the melt at 1200
1555 K. B) The dependence of the compressibility of a melt-crystal-volatile mixture on the crystal
1556 content of the melt. As the magma cools and crystallises, the melt becomes volatile-saturated and
1557 the compressibility rapidly increases beyond that for the solid rock. Curves are shown for melt
1558 with a H_2O content of 3, 4 and 6 wt%, in a reservoir of depth 5 km, with magma temperature
1559 varying with the crystal content of the melt. C) Rate of change of the reservoir pressure during
1560 second boiling as a function of the change in temperature, normalised to the critical pressure
1561 required to trigger an eruption, here taken to be 10 MPa (Blake, 1984). Curves are shown for H_2O
1562 contents of 3, 4 and 6 wt%.
1563

1564 **Figure 6**. Data on the cumulative mass erupted from (A) Soufriere St Vincent and (B) Paracutin,
1565 as a function of time, compared to the exponential model for the gradual waning of the eruption
1566 rate; (C) Lanquimay, compared to a model for the mass erupted from a two magma chamber
1567 system, with the dashed line illustrating the erupted mass from the deeper chamber into the upper
1568 chamber, and the black line the erupted mass from the upper chamber to the surface. The lower
1569 chamber only starts to supply a significant flux of magma once the upper chamber has
1570 decompressed. (D) May St Helens, after May 18 1980 until 1985. Here the symbols represent the
1571 incremental erupted volume during successive dome explosion events; the black line is a model
1572 with an idealized steadily waning eruption rate and the dashed line is the model in which each
1573 explosive event occurs once a prescribed overpressure has been reached (for details see
1574 (Berkowitz and Woods, 2018 under review)).
1575

1576 **Figure 7:** Illustration of the process of overturn associated with volatile exsolution from a melt
1577 prior to an eruption. A: the lower layer of melt is deep and viscous, leading to a dominant plume
1578 of bubble-rich buoyant melt rising up through the overlying volatile poor melt, leading to large
1579 scale overturn. B: the lower layer is less viscous and shallower, leading to smaller plumes of
1580 bubble-laden buoyant melt rising up into the overlying layer of volatile-poor melt. These plumes
1581 become unstable and are mixed into the overlying layer of melt rather than leading to a dominant
1582 overturn event (Woods and Cowan, 2009). The vertical scale of the experiments is ~ 20 cm.
1583

1584 **Figure 8**. Overturn during an eruption, as the lower layer of volatile-rich melt expands and
1585 becomes less dense than the original upper layer. This leads to a change in the erupting melt
1586 issuing from the summit 'vent' and the flank 'vent' following the overturn (Experiment courtesy
1587 of Alex Cowan). The vertical scale of the experimental tank is ~ 20 cm.

Figure 9: Results of experiments to show the exsolution of gas in a particle-laden viscous polymer solution as the solution is decompressed. Top: sequence of images showing the solution during and after decompression from 1 Bar to 35 mBar, leading to (i) exsolution of gas, (ii) liquid displacement within the pack and some dilation of the porous pack, producing an increase in permeability of the pack, (iii) the development of channelised permeable flow of gas from the pack; (iv) gradual relaxation of the depth of the porous layer once the connected gas phase has been driven out of the system. The tank is 18.2 cm wide. Owing to presence of residual gas, and the original expulsion of some liquid from the pack, a thin layer of melt may be seen above the porous pack (light layer at top of pack). Bottom: Graph illustrating the height of the particle-laden solution as a function of time when the pack is subjected to a decompression to different final pressures, as shown in the legend. With high final pressure, the effect is a monotonic increase in depth, as there is less gas exsolved. With a low final pressure the effect is a much larger increase in depth during the initial exsolution, but then the pack relaxes as gas is able to escape from the system. After Ptacek et al., sub judice (2018).

Figure 10: Cartoon diagram to summarise the generation, transport and accumulation mechanisms of the exsolved volatile phase, and the ways in which the exsolved volatile phase plays a role in driving magma mingling and mixing involving underplating mafic magmas.

A: Exsolution of volatiles during decompression, “first boiling”

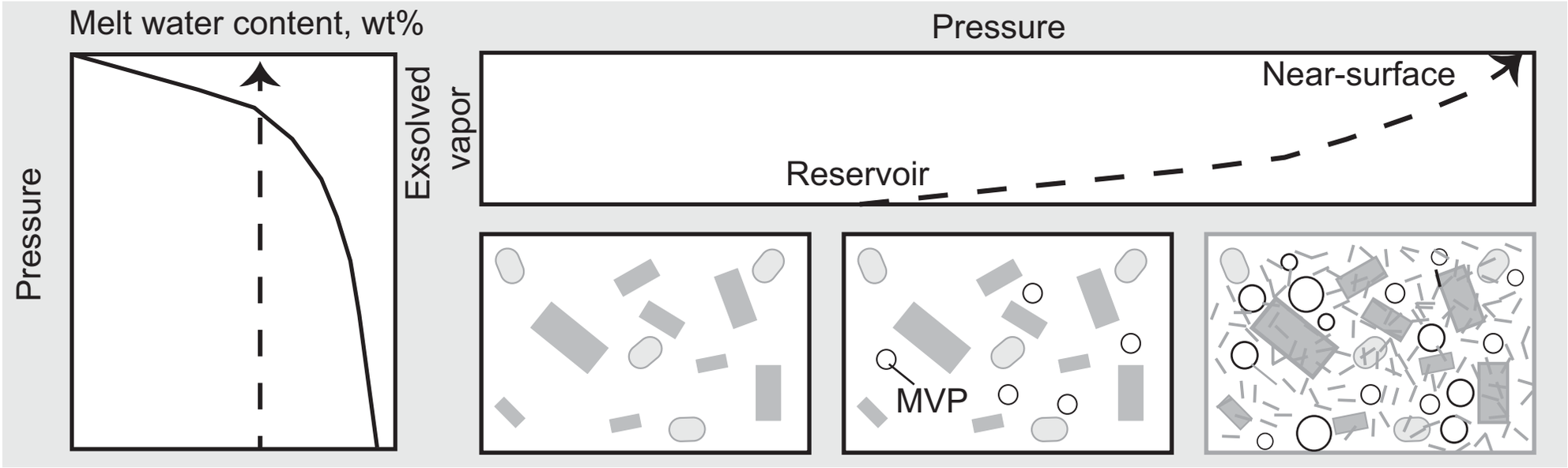

B: Exsolution of volatiles during cooling and crystallisation, “second boiling”

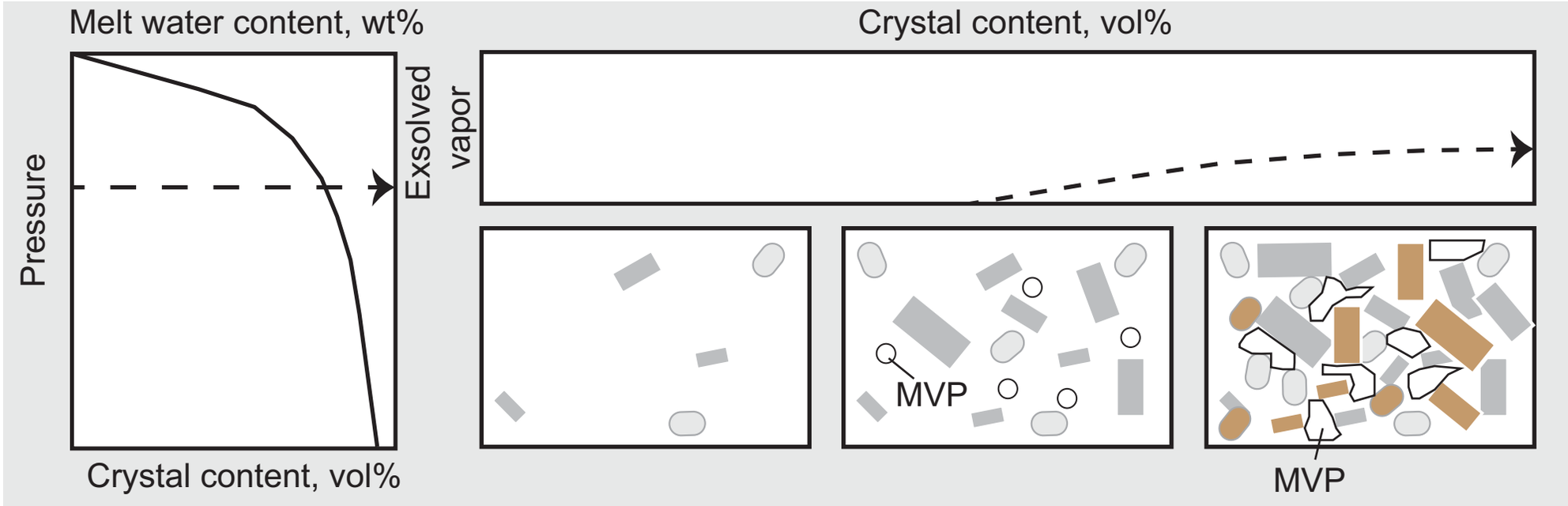

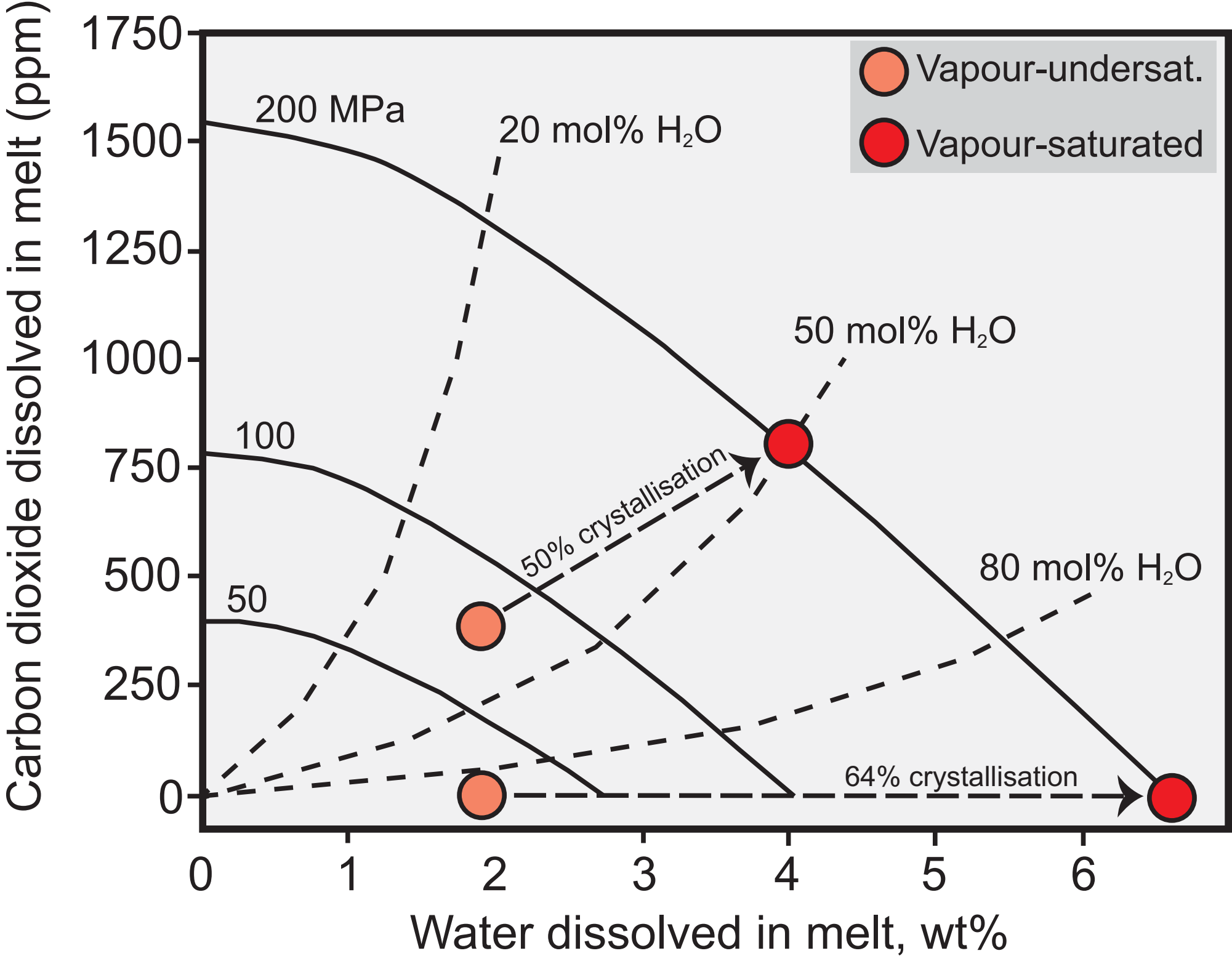
Carbon dioxide dissolved in melt (ppm)
1750
1500
1250
1000
750
500
250
0
0
1
2
3
4
5
6
Water dissolved in melt, wt%
Vapour-undersat.
Vapour-saturated
200 MPa
100
50
20 mol% H2O
50 mol% H2O
80 mol% H2O
50% crystallisation
64% crystallisation

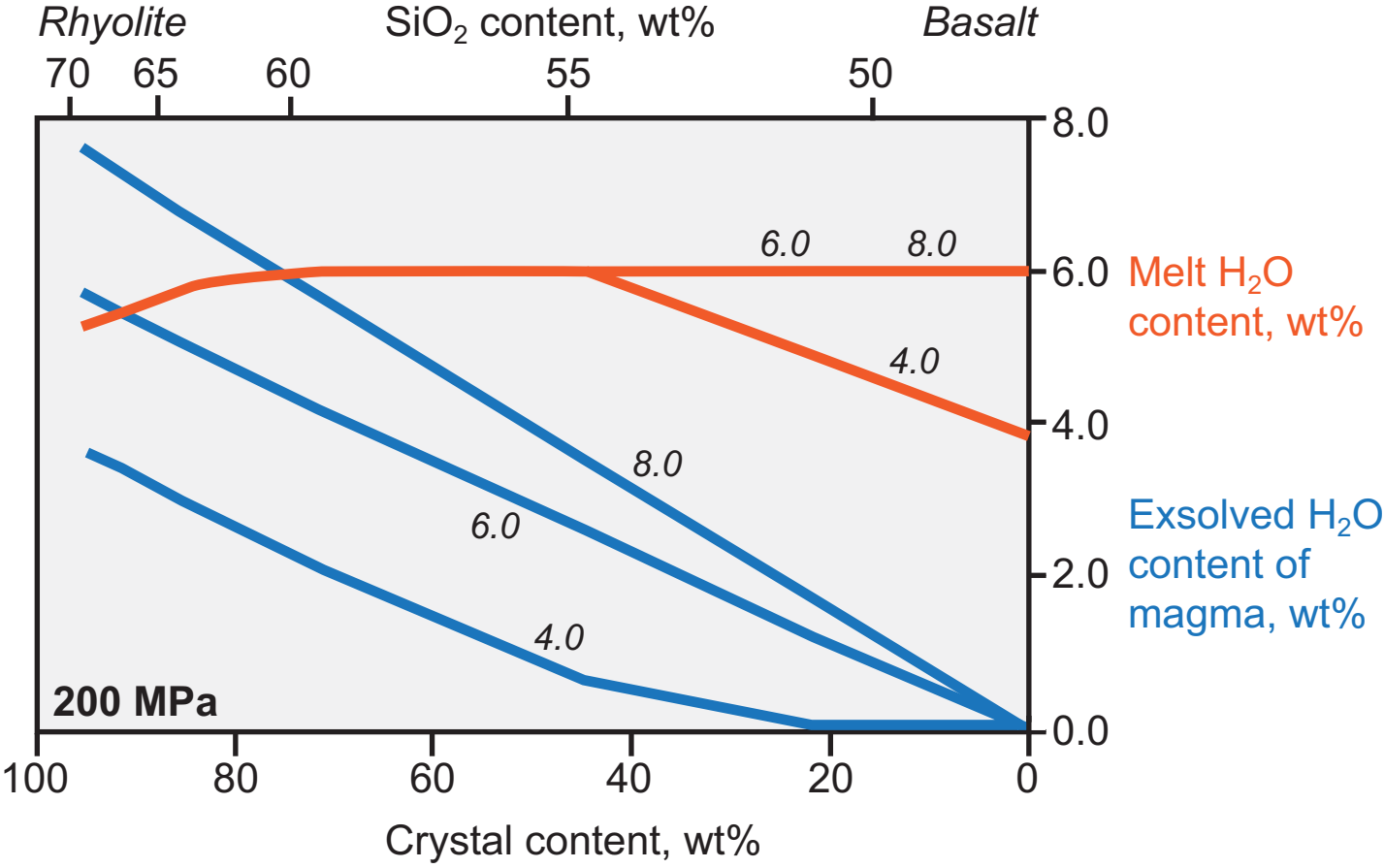
Rhyolite
SiO2 content, wt%
Basalt
70
65
60
55
50
8.0
6.0
4.0
2.0
0.0
6.0
8.0
4.0
8.0
6.0
4.0
200 MPa
Melt H2O content, wt%
Exsolved H2O content of magma, wt%
100
80
60
40
20
0
Crystal content, wt%

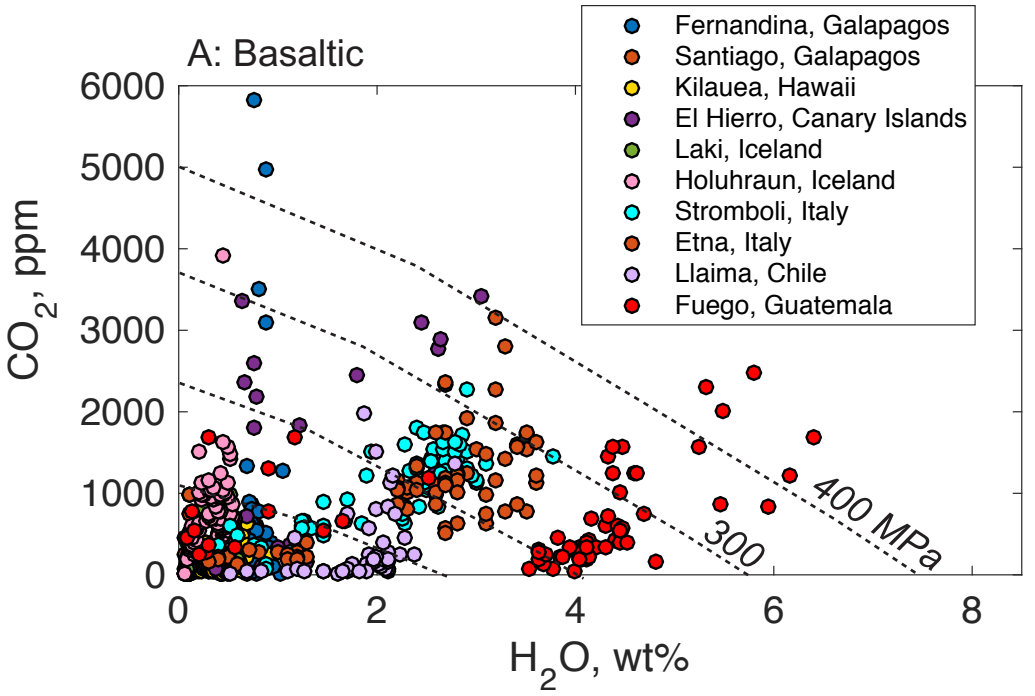
A: Basaltic
Fernandina, Galapagos
Santiago, Galapagos
Kilauea, Hawaii
El Hierro, Canary Islands
Laki, Iceland
Holuhraun, Iceland
Stromboli, Italy
Etna, Italy
Llaima, Chile
Fuego, Guatemala
400 MPa
300
CO2, ppm
H2O, wt%
0
1000
2000
3000
4000
5000
6000
0
2
4
6
8

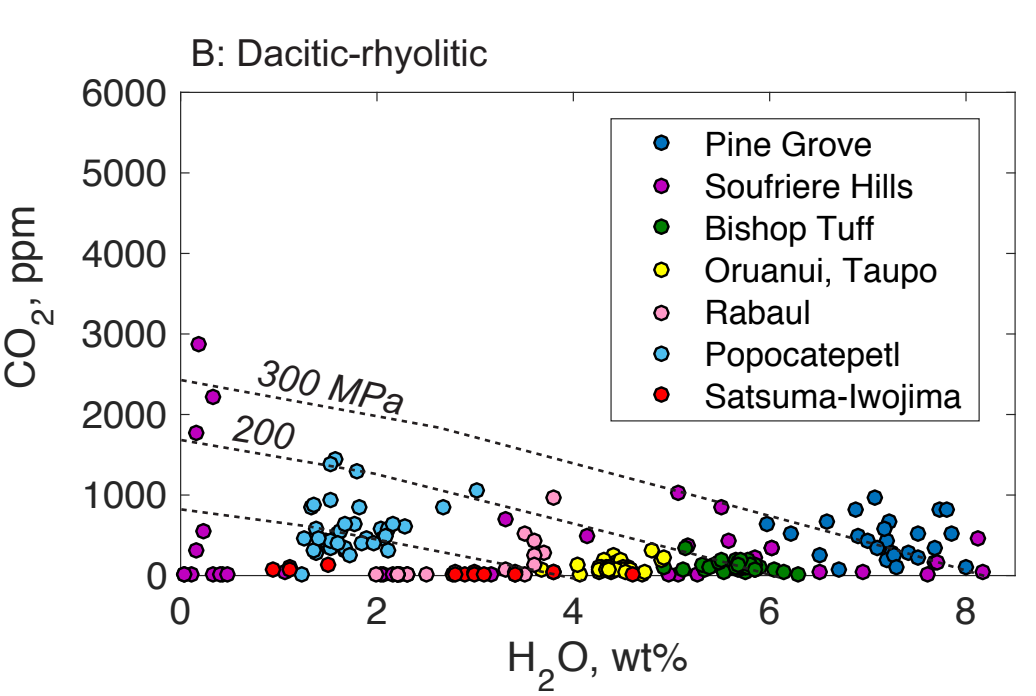
B: Dacitic-rhyolitic
Pine Grove
Soufriere Hills
Bishop Tuff
Oruanui, Taupo
Rabaul
Popocatepetl
Satsuma-Iwojima
300 MPa
200
CO2, ppm
H2O, wt%
0
1000
2000
3000
4000
5000
6000
0
2
4
6
8

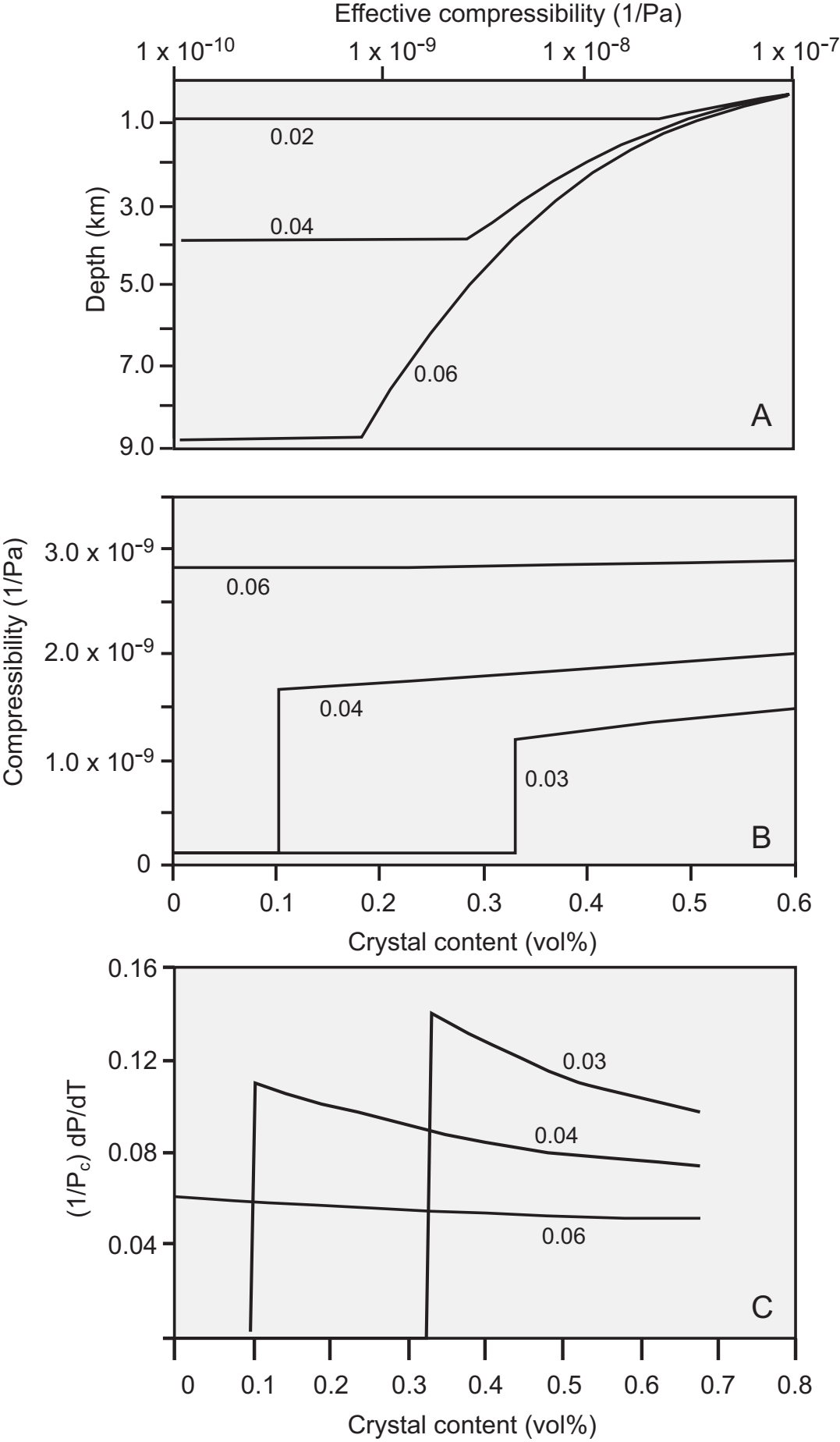
Effective compressibility (1/Pa)
1 x 10-10
1 x 10-9
1 x 10-8
1 x 10-7
Depth (km)
1.0
3.0
5.0
7.0
9.0
0.02
0.04
0.06
A
Compressibility (1/Pa)
3.0 x 10-9
2.0 x 10-9
1.0 x 10-9
0
0.06
0.04
0.03
B
0
0.1
0.2
0.3
0.4
0.5
0.6
Crystal content (vol%)
(1/Pc) dP/dT
0.16
0.12
0.08
0.04
0.03
0.04
0.06
C
0
0.1
0.2
0.3
0.4
0.5
0.6
0.7
0.8
Crystal content (vol%)

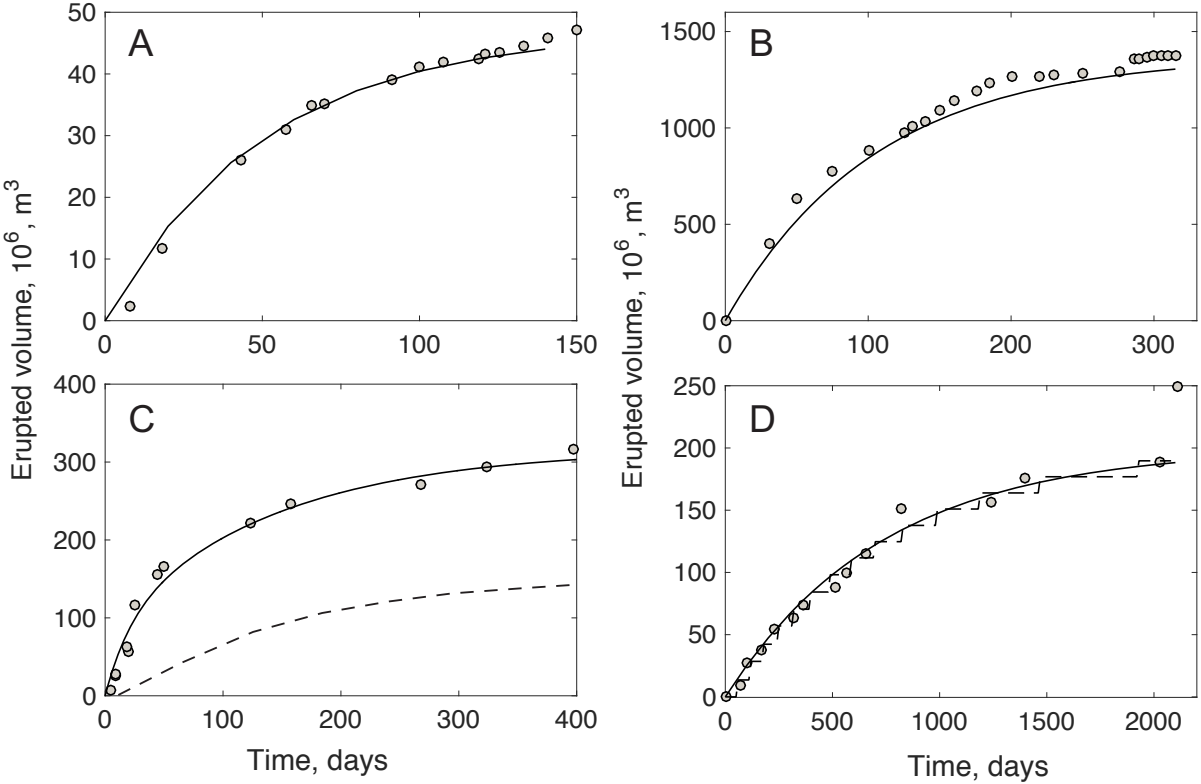
A
B
C
D
Erupted volume, 10^6, m^3
Erupted volume, 10^6, m^3
Time, days
Time, days
0
10
20
30
40
50
0
50
100
150
0
500
1000
1500
0
100
200
300
0
100
200
300
400
0
100
200
300
400
0
50
100
150
200
250
0
500
1000
1500
2000


A


B

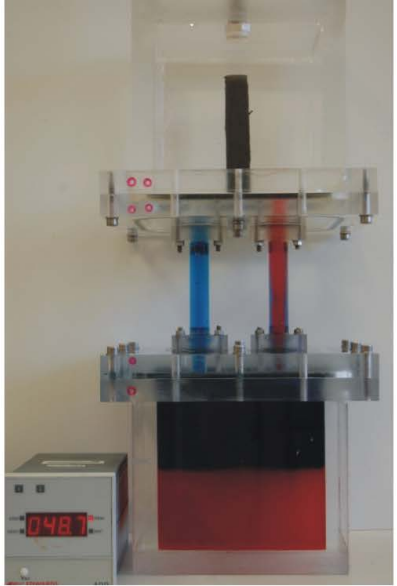
0481

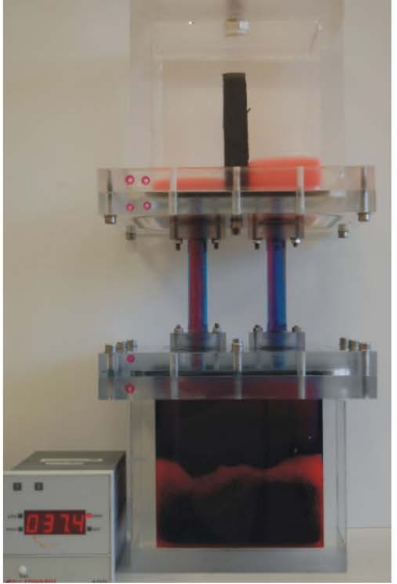
0374

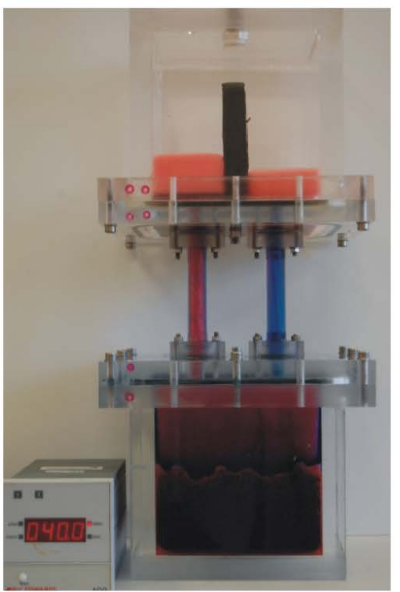
0400

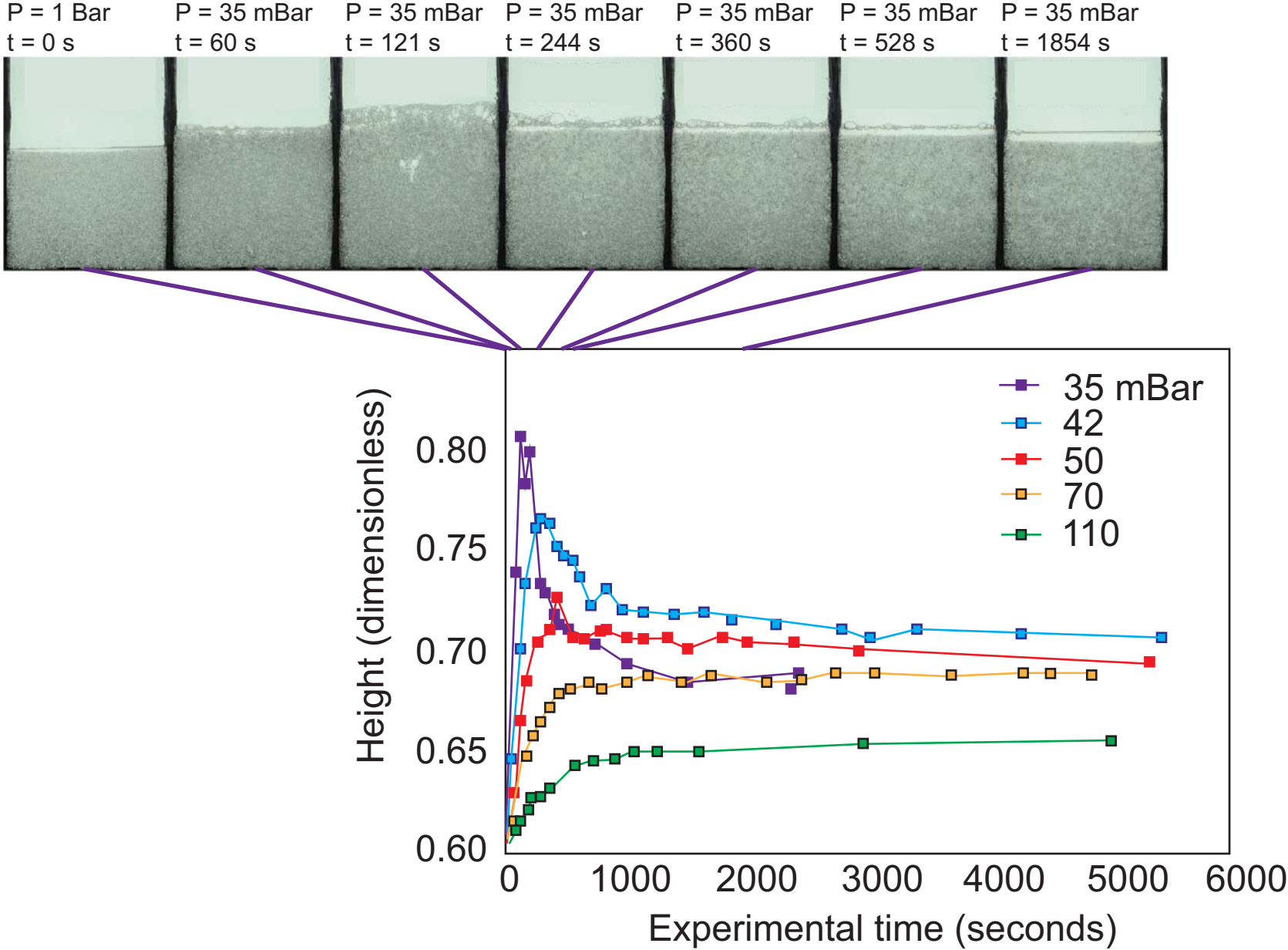
P = 1 Bar
t = 0 s
P = 35 mBar
t = 60 s
P = 35 mBar
t = 121 s
P = 35 mBar
t = 244 s
P = 35 mBar
t = 360 s
P = 35 mBar
t = 528 s
P = 35 mBar
t = 1854 s
35 mBar
42
50
70
110
Height (dimensionless)
0.80
0.75
0.70
0.65
0.60
0
1000
2000
3000
4000
5000
6000
Experimental time (seconds)

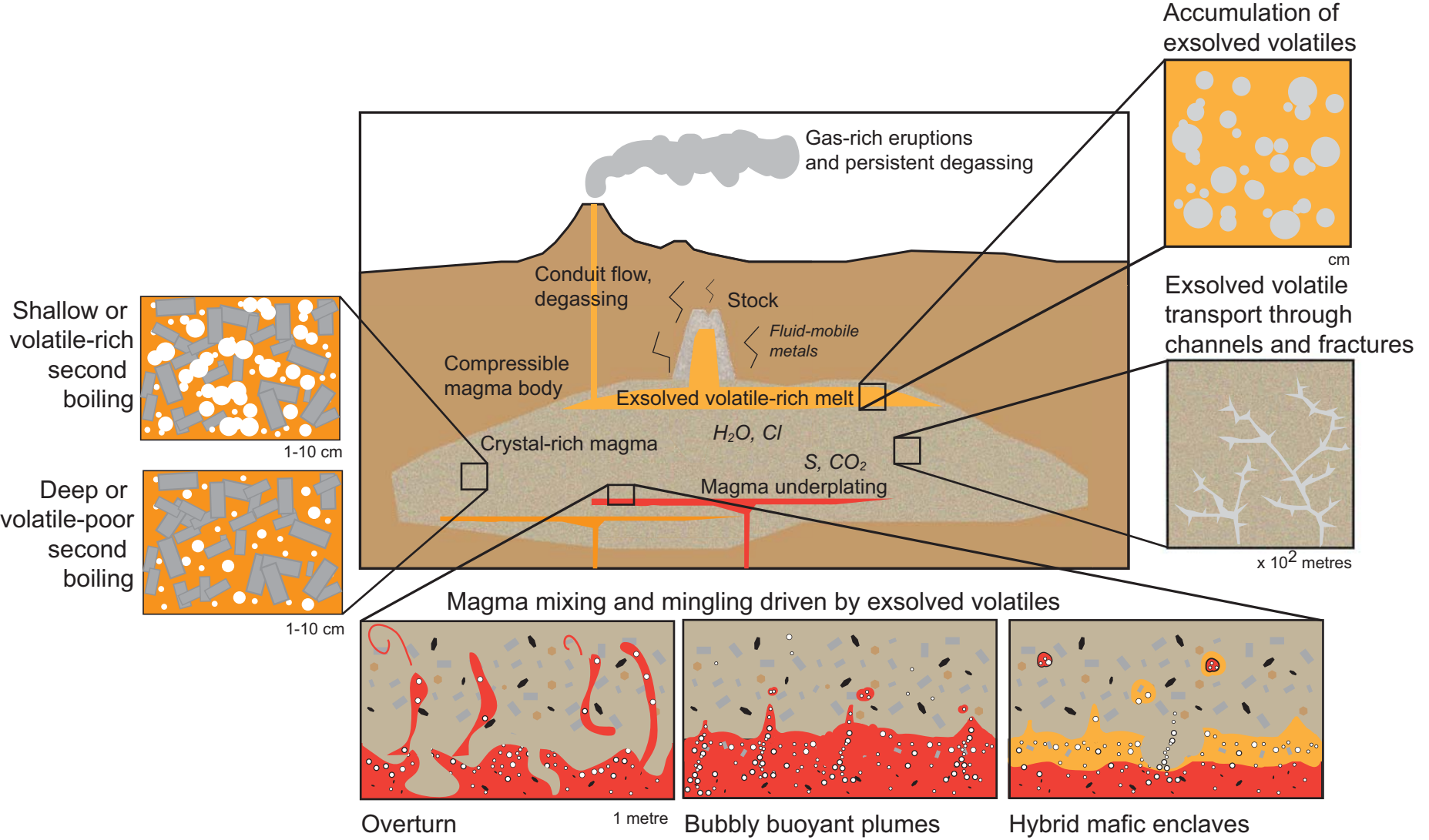
Accumulation of exsolved volatiles
cm
Gas-rich eruptions and persistent degassing
Conduit flow, degassing
Stock
Fluid-mobile metals
Compressible magma body
Exsolved volatile-rich melt
H_2O, Cl
Crystal-rich magma
S, CO_2
Magma underplating
Exsolved volatile transport through channels and fractures
x 10^2 metres
Shallow or volatile-rich second boiling
1-10 cm
Deep or volatile-poor second boiling
1-10 cm
Magma mixing and mingling driven by exsolved volatiles
Overturn
1 metre
Bubbly buoyant plumes
Hybrid mafic enclaves